A STUDY OF HIGH-K DIELECTRIC MATERIALS IN CONJUNCTION WITH A MULTILAYER THICK-FILM SYSTEM
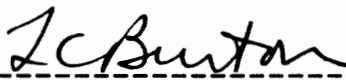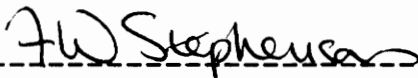
BY

RAJ REDDY

Thesis submitted to the Faculty of the

Virginia Polytechnic Institute and State University

in partial fulfillment of the requirements for the degree of

Master of Science
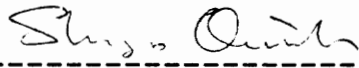
in

Electrical Engineering

APPROVED:

L. C. Burton, Chairman

F. W. Stephenson, Co-chairman   S. Onishi

May, 1988

Blacksburg, Virginia

A Study of High-K Dielectric Materials in Conjunction with a
Multilayer Thick-film system

by

Raj Reddy

Electrical Engineering

(ABSTRACT)

A new family of dielectric materials has been studied,
individually as thick-film capacitors and as buried
components incorporated in second-order lowpass and bandpass
RC active filter circuits. The materials were electrically
characterized in terms of the variation of dielectric
constant and dissipation factor with frequency. The
performance of the filter circuit is related to the
characteristics of the dielectric materials. An analysis of
the circuit is developed which accounts for the capacitor
losses.

ACKNOWLEDGEMENTS

TABLE OF CONTENTS

Table of contents   v

LIST OF FIGURES

LIST OF TABLES

CHAPTER 1. INTRODUCTION

1.1 Introduction

Recent advances in thick film dielectric materials have attracted renewed interest in employing these materials to fabricate high value capacitors [1]. Invariably, these new dielectrics contain barium-titanate as the major constituent. Improvements in the glass-binder used have also helped in the reduction of the porosity of these dielectric materials as well as improving the compatibility between the conductor and dielectric layers [2,3].

Thick film capacitors fabricated are in direct competition with chip capacitors which provide much higher values of capacitance as well as greater reliability. The advantage of thick film capacitors over chip capacitors is achieved only when they are buried under a multilayer dielectric leaving the top area for the conductor pattern and other devices. Also, thick film capacitors provide far better thermal matching with the alumina substrate than do chip capacitors.

1.2 Objectives

A set of high-K (K=100, 300, 1000) and associated low-K dielectric materials (K=10, 20, 50), all of which fire at

980°C were developed by Engelhard Industries. These materials were available at the start of the research program. Preliminary studies at Engelhard indicated that the above systems were compatible, thereby suggesting the possibility of using the two sets in a single multilayer structure. In this way, high-K materials can potentially be used to form capacitors which are buried within the structure without sacrificing the upper layer surface area needed for resistors and active devices.

The main objectives of this research are to examine the properties of buried capacitors in an actual working circuit and, subsequently, the properties of the circuit. The devices were investigated as part of an active RC filter circuit whose performance parameters were then related to the quality of the capacitors.

In order to carry out these objectives, initial studies concentrated on the performance of individual capacitors, using the new dielectric materials, prior to the fabrication and testing of a multilayer circuit.

1.3 Proposed tests

The new materials, most of which are barium-titanate based were characterized by the following measurements: (i) dielectric constant vs frequency (5 Hz-10 MHz), and temperature (25°C-125°C);

(ii) dissipation factor vs frequency (1 KHz and 10 KHz);
      insulation resistance at room temperature, at a test
      voltage of 10 V and testing time of 1 minute;

(iv) leakage current vs voltage and temperature;

(v)   conductance vs frequency (5 Hz-10 MHz);

(vi) film porosity, topography and uniformity, and their
      bearing on silver migration using SEM, ESCA and EDAX.

The major research objectives of this thesis are,
therefore, to electrically characterize available dielectric
materials by means of the indicated techniques, and then to
study the use of thick film capacitors as components in
active filter circuits, with modelling of their accompanying
losses.

CHAPTER 2. LITERATURE REVIEW

2.1 Barium titanate

In order to yield maximum capacitance per unit area, capacitor materials must have as high a dielectric constant as possible. The most widely used material is barium titanate ($BaTiO_3$). This is a ferroelectric material which has a dielectric constant very strongly dependent on temperature, rising quite sharply to a peak value of around 10,000 at the Curie temperature of 120°C, above which it falls off rapidly [4,5]. The position of this peak can be moved along the temperature axis by incorporating structurally similar compounds such as lead or strontium titanates [6,7], but the rapid variation of dielectric constant with temperature still makes the material impractical for capacitor applications. The variation is reduced to acceptable proportions by the addition of small percentages of "depressors" or temperature compensators which flatten the peak to the extent that the dielectric constant varies by only a factor of about two over the useful working temperature range, e.g., 500-1000.

2.2 Barium titanate capacitor dielectrics

$BaTiO_3$ is a ferroelectric. Such materials are similar

to ferromagnetics in that they exhibit spontaneous polarization hysteresis, a domain structure, and wall displacement below a Curie temperature, T_C. The primary polarization process arises from a displacement of the mean center of the positive ions in the crystal lattice with respect to the mean center of the negative ions. In the dielectric state, all perovskites are cubic; below the Curie temperature they are tetragonal or rhombohedral. $BaTiO_3$ is tetragonal below 120 to $130^O C$, depending on purity and particle size. In the spontaneously polarized state the crystal has a dielectric constant of the order of several hundred since it can be further polarized by an externally applied field [7,8].

When a ferroelectric ceramic is used as a dielectric in a capacitor, the requirements of high dielectric constant and low loss must be satisfied. In barium titanate, these are both met by producing a microstructure with small grains which suppress the ferroelectric behaviour [6,8]. When the crystal changes from the dielectric to the ferroelectric state, there is a stiffening of the lattice in the direction which becomes the polar axis. The positive and negative ions then become less easy to displace with respect to one another. As a consequence, the dielectric constant in coarse-grained material with grain size of 50 to 100 microns is relatively low [6,7]. When the ceramic is cooled, the value decreases from about 10,000 at the Curie point to 1000

at room temperature.

2.3 RC Active filters

Active RC filters have been used to satisfy analog
applications in the electronics and communications
industries for the past twenty years [10]. This has been
brought about largely by significant improvements in the
performance and cost of sophisticated miniature operational
amplifiers made with active silicon devices, as well as the
reduced size and relatively low cost of RC hybrid (laser-
trimmed) circuits.

Many active filters have been fabricated using tantalum
thin film technology. Such circuits are typically comprised
of tantalum thin-film resistors and tantalum capacitors with
operational amplifiers as add-on component [9]

It is well known that thick-film capacitors offer a
high unit capacitance for a film technology, increased
hybrid design capability, a potential increase in
reliability, and cost advantages. Their disadvantages
include poor physical properties, limited electrical
properties, and complex processing.

Because of these reasons, most examples of thick-film
hybrid RC active filters found in the literature use chip,
rather than screened, capacitors. Reference [10] describes
a low cost thick-film RC network using a glass-film

passivation system to protect the thick-film capacitors. Unless passivated, problems arise during high humidity when capacitors are shorted. It has also been reported that attempts to increase capacitance by firing to higher temperatures, to achieve denser dielectric layers, led to lower dielectric strength and an increased number of shorts. Thinner dielectric layers also led to the same problems. In such cases, the extent to which miniaturization is carried is limited due to the large area being occupied by the thick-film capacitors.

In the following chapters, a method is evolved to alleviate the above mentioned problem by burying the capacitors in a multilayer structure. An analysis is provided which takes into account the losses of the capacitors in the circuit.

CHAPTER 3. MATERIALS AND METHODS

3.1 Materials

The materials for this research were provided by Engelhard Corporation, and included conductor, resistor, dielectric and overglaze compositions for incorporation in a multilayer circuit. These are experimental materials and are not commercially available at the present time.

3.1.1 Conductor

Two conductor pastes were provided viz. Ag/Pd (70:30) and Au. Both compositions gave good printed resolution and were fired at the recommended $980^{\circ}C$ with 10 minutes at the peak and a total cycle time of 60 minutes. The materials were found to give good adhesion to the substrate and had high wettability for the purposes of soldering with 62% Sn 36% Pb and 2% Ag. Ag/Pd was not wire bondable either with gold or aluminum wire despite removal of the oxide layer formed. Gold gave excellent bondability with wire of 2 mil diameter.

3.1.2 Dielectrics

Dielectric compositions ranged from K=6 to K=1000. One

TABLE 1.   Notation for each dielectric material, and

its insulation resistance

Notation	Dielectric Constant	Insulation Resistance
A 4877	10	$0.4 \times E11$ Ω
A 4878	20	$1.0 \times E11$ Ω
A 4842	50	$1.4 \times E11$ Ω
A 4879	100	$1.1 \times E11$ Ω
A 4880	300	$1.0 \times E11$ Ω
A 4881	1000	$1.6 \times E11$ Ω

Materials and methods

of the objectives of this research program was to electrically characterize these materials. Table 1 indicates the notation used for each dielectric paste as well as the various dielectric constants. The high-K dielectrics are barium-titanate based.

3.1.3 Resistors

The resistor pastes provided have been successfully utilized for a number of years and are of high reliability [11,12]. These are ruthenium-oxide based and Table 2 indicates the sheet resistivities of each type on alumina substrates as well as on a multilayer dielectric.

3.2 Design
3.2.1 Thick-film capacitor

The thick-film capacitors were designed using a computer-aided-design (CAD) software package developed in the Hybrid Microelectronics Laboratory. Figure 1 shows the layout of the thick-film capacitor. While designing the capacitors, the following guidelines were adhered to:

(i) screened dielectric overlapped the lower electrode by a minimum of 10 mils on each side,

(ii) the top electrode fell completely within the bottom electrode area.

TABLE 2. Notation and properties of resistors used in study

-

Resistor notation	Sheet resistivity alumina	dielectric	firing temperature
A 3604	10 KΩ/▪	3.4 KΩ/▪	850°C
A 3605	100 KΩ/▪	45 KΩ/▪	850°C

dielectric   Bottom electrode

Top electrode
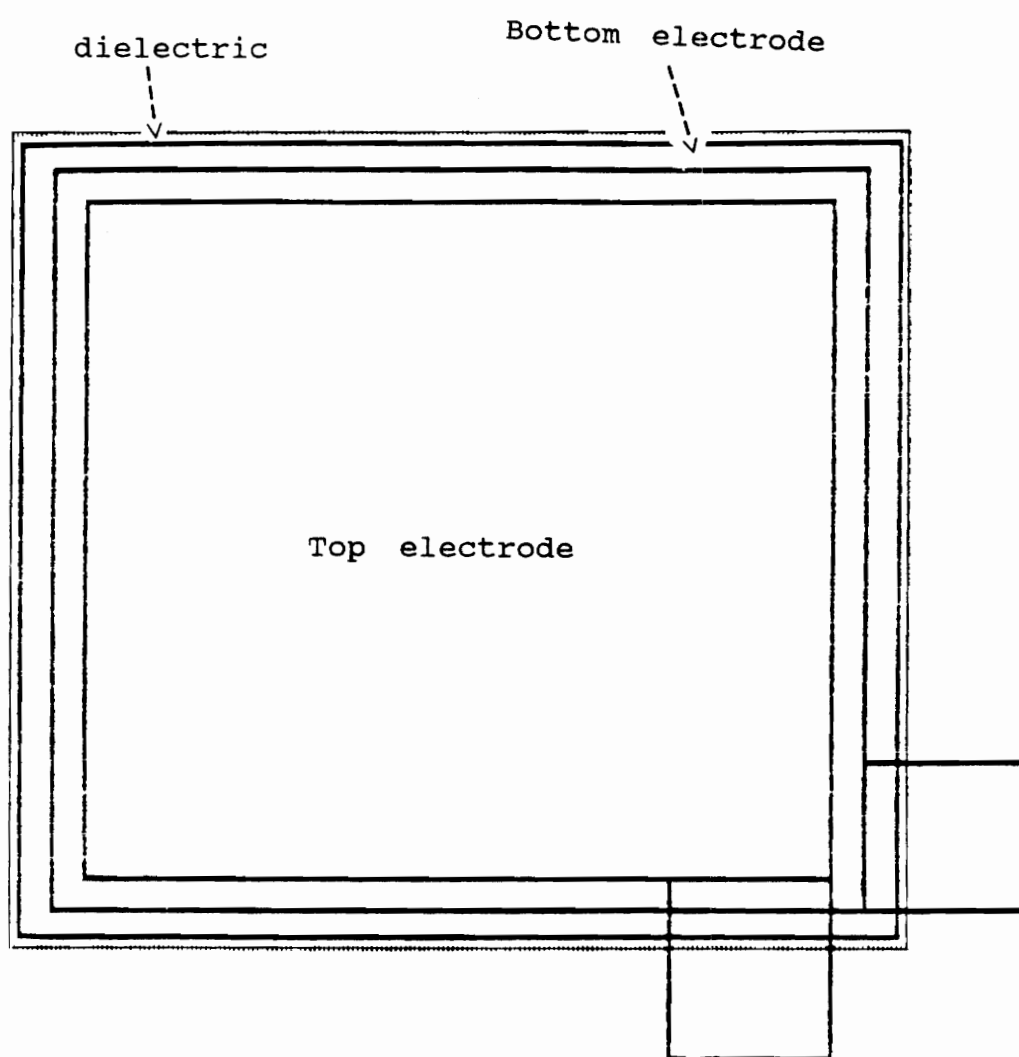
Figure 1.   Layout of thick-film capacitor

Materials and methods   12

TABLE 3. Differences between lowpass and bandpass RC active filter circuits

.

Circuit type	Lowpass	Bandpass
# of firings	13	8
cross-overs	one	none
wire-bonding	yes	no
center frequency	750 Hz	5000 Hz
quality	5	15
high-k material	300, 1000	300, 1000
low-K material	10, 20, 50	none

3.2.2 Thick-film hybrid microcircuit

Two RC active filter circuits were designed using the CAD package. The particulars of each circuit are given in Table 3.

The pattern for the lowpass filter was designed so as to yield capacitors with an area ratio of 4:1. These were designed on the bottom layers which were then encapsulated with a multilayer dielectric A 4834. In effect, the capacitors were buried under this glaze. The layer on top of the dielectric was designed to accommodate resistors, an operational amplifier (LF 351 M) and upper conductor pattern. Vias were designed in the dielectric layer to provide interconnection between the top and the bottom layers. In this case, a cross-over could not be avoided. A schematic of each of the layers, and a composite, is shown in Figure 2. The resistors were designed for an untrimmed value of 80% nominal. The circuit diagrams of both the lowpass and the bandpass filter are shown in Figure 3. The thick-film layout of the bandpass filter circuit is illustrated in Figure 4.

3.3 Process sequence
3.3.1 Thick-film capacitor

First, the bottom electrode was printed, settled, dried
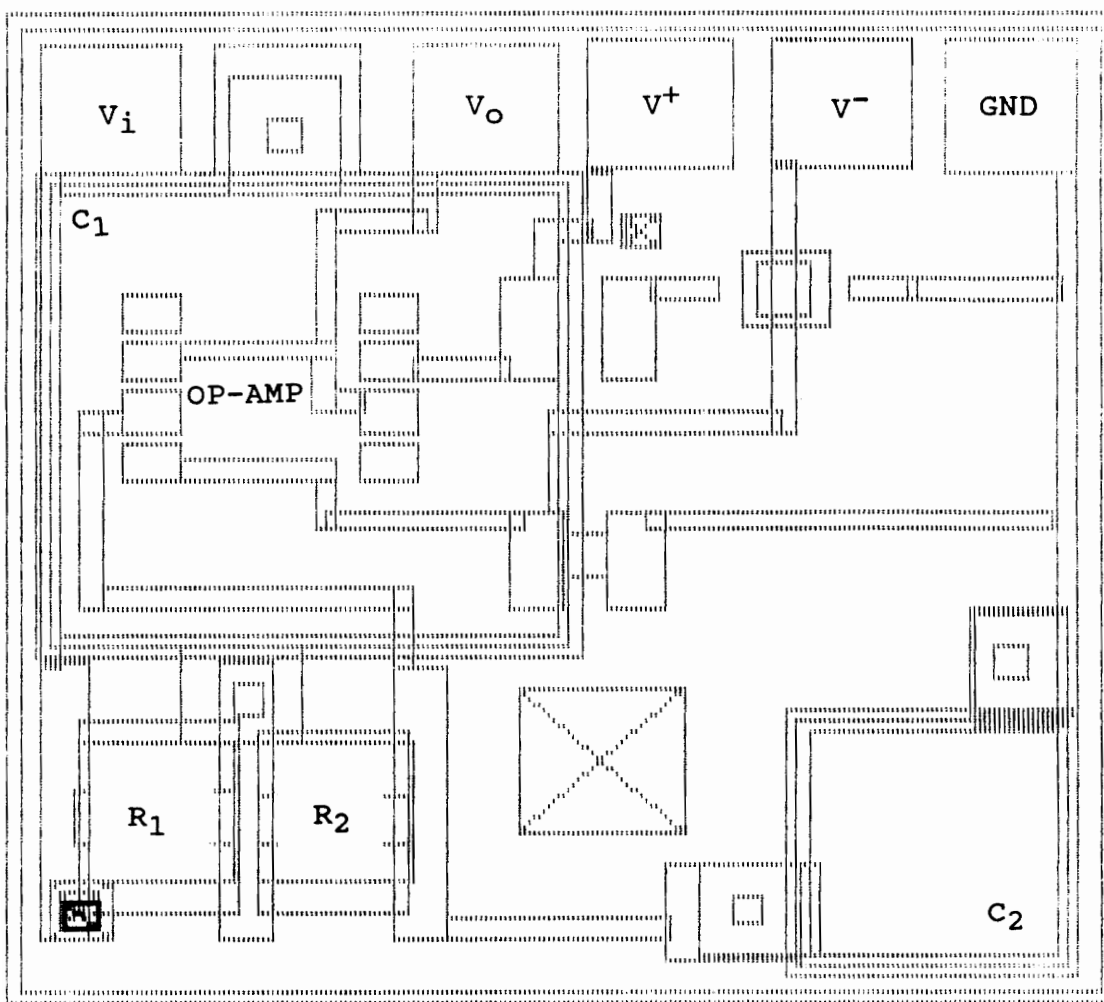
Figure 2. Thick-film schematic of lowpass RC active
            filter circuit

Materials and methods   15
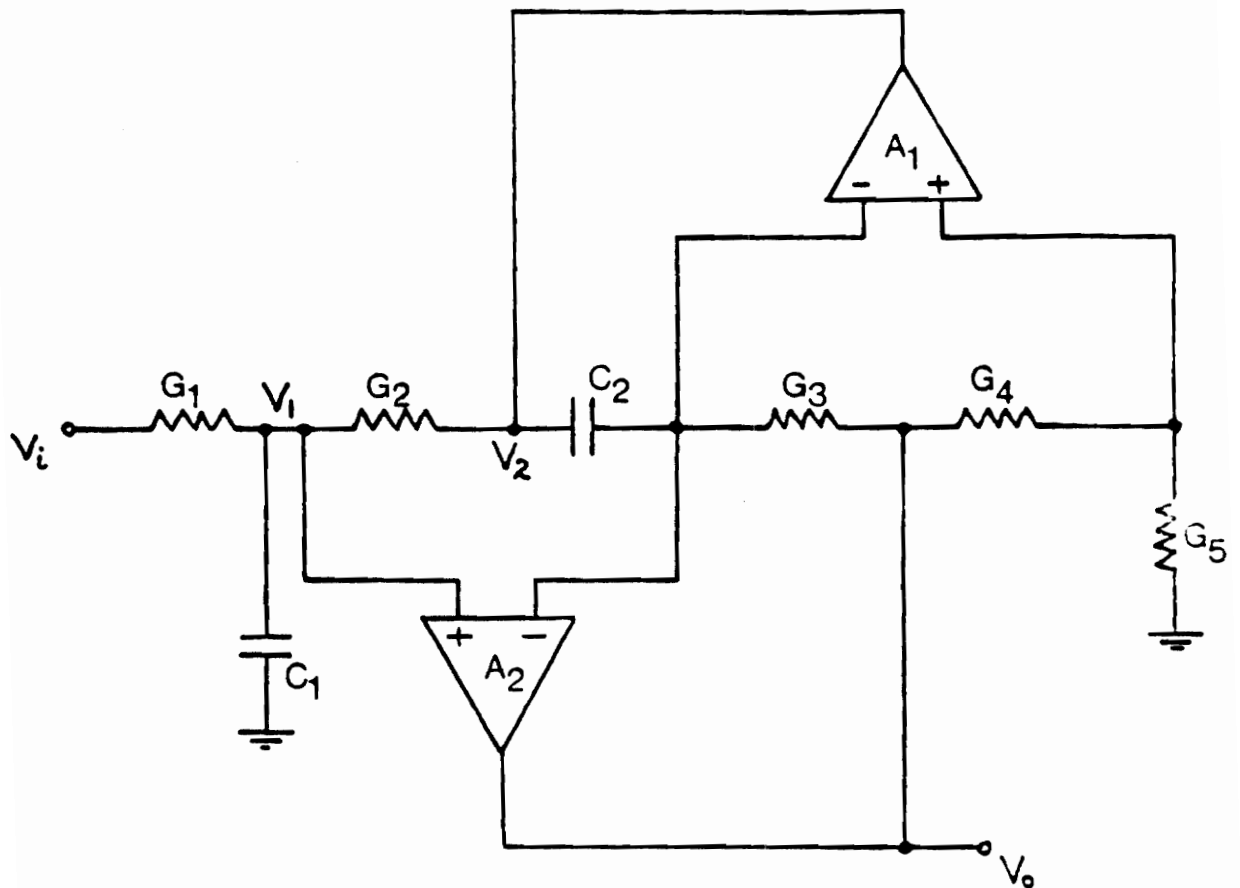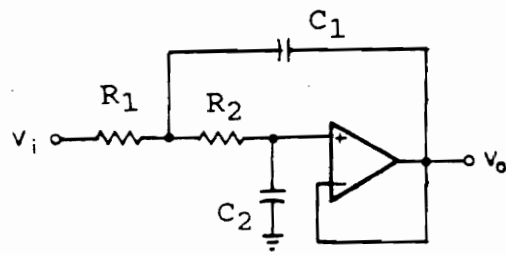
Figure 3. Circuit diagrams of lowpass and bandpass RC active filter

Materials and methods
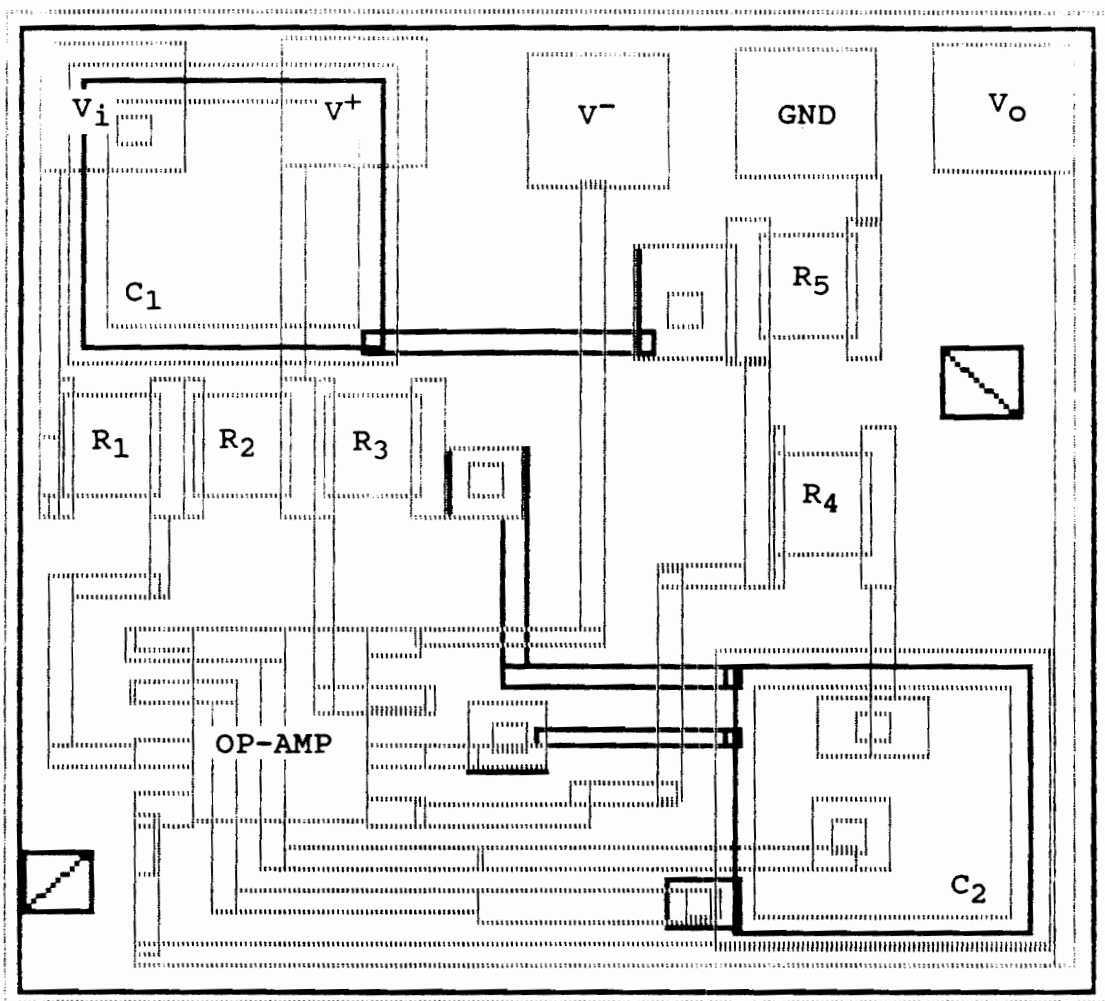
Figure 4.   Thick-film schematic of bandpass RC active filter
circuit

Materials and methods   17

and fired and then the dielectric was screened on top of the bottom electrode. This was done three times so as to prevent the occurence of shorts due to the porosity of the material. Each of the layers, was fired separately. A number of capacitors were fabricated using the above method. The set was then divided in two halves. One half was set aside while the other half was printed with two more layers of overglaze. Hence, it was later possible to study the difference an overglaze makes on the value of a capacitor.

3.3.2 Hybrid microcircuit

The two capacitors to be buried under the multilayer dielelectric were fabricated with two different dielectric materials. The large area capacitor consisted of a high-K dielectric and the small capacitor a low-K dielectric. This was carried out in order to prove that, as the high-K capacitors were of lower quality, they would play a dominant role in the performance of the circuit.

After the fabrication of capacitors, they were buried using the multilayer dielectric A 4834. Vias were allocated for the connection to the upper conductor layer. Square vias of dimensions 30 mil by 30 mil were used. The multilayer dielectric was double printed separately to reduce pinhole formation. The top conductor was printed after burying the capacitors with the multilayer dielectric.

A slow squeegee speed was used to ensure that all the vias were filled with conductor material. The resistors were then printed, dried and fired. To bring the resistors to their nominal values, an abrasive trimmer was used to achieve a tolerance of less than 1%. Finally, the operational amplifier was attached using reflow solder. To eliminate the operational amplifier from affecting the response of the circuit a high gain-bandwidth product was needed. This was achieved by using National Semiconductor's LF 351 M. Table 4 provides additional information on the various factors of importance to subsequent discussions.

3.4 Microscopy and compositional analysis

Characterization of the microstructure was performed on an AMR 900 scanning electron microscope. The composition of the material was determined on the same machine by using an EDAX 9100 energy dispersive analyzer. The dielectric samples were coated with carbon to improve the surface conductivity for examination in the scanning electron microscope. SEM pictures were taken of the cross-sectioned samples.

TABLE 4. Key factors for screen printing

.

Conductor screen	325 stainless steel
dielectric screen	250 stainless steel
resistor screen	250 stainless steel
squeegee	90 durometer
breakaway distance	25 mils
emulsion	1 mil
solder	62% Sn, 36% Pb, 2% Ag

CHAPTER 4. MEASUREMENT AND RESULTS

4.1 Microstructure

The topography of the samples were studied using an SEM as outlined in Section 3.4. Figures 5-10 show photographs of dielectric pastes with K ranging from 10 to 1000. They all indicate a certain amount of porosity although no obvious trend is apparent. Figure 5 shows an SEM picture of the Pd/Ag electrode surface. After performing EDAX on high-K samples, it is seen that these predominantly contain barium, titanium and lead. EDAX analyses of the samples are shown in Figures 11-14.

4.1.1 K=100 dielectric

For samples containing this dielectric, it was found that the top electrode layer contained blisters. Some of these bubble-like structures are ruptured, as seen at a magnification of X 500. This is attributed mainly to the incompatibility of this particular dielectric with Pd/Ag conductor paste. Also, the gases formed were unable to escape during firing. The bubble formation was absent when Au was used as the conductor paste.
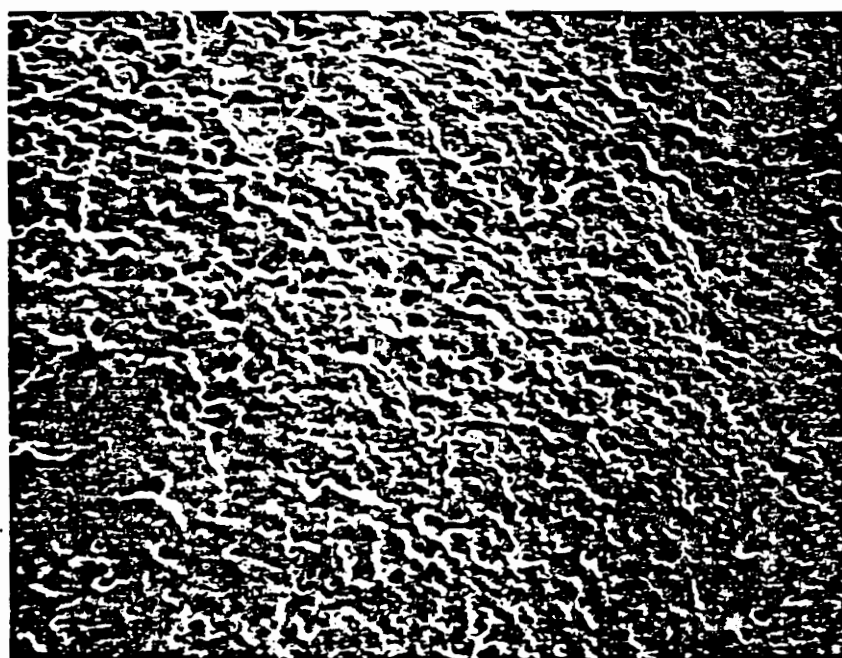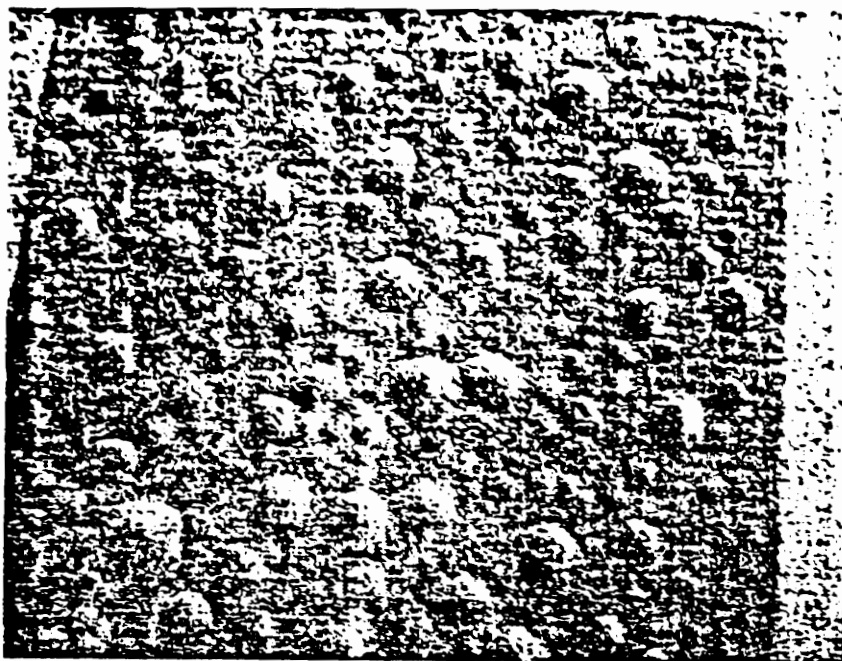
Figure 5.   SEM micrographs of top electrode (Pd/Ag)
            X20 (top) and X500 (bottom)
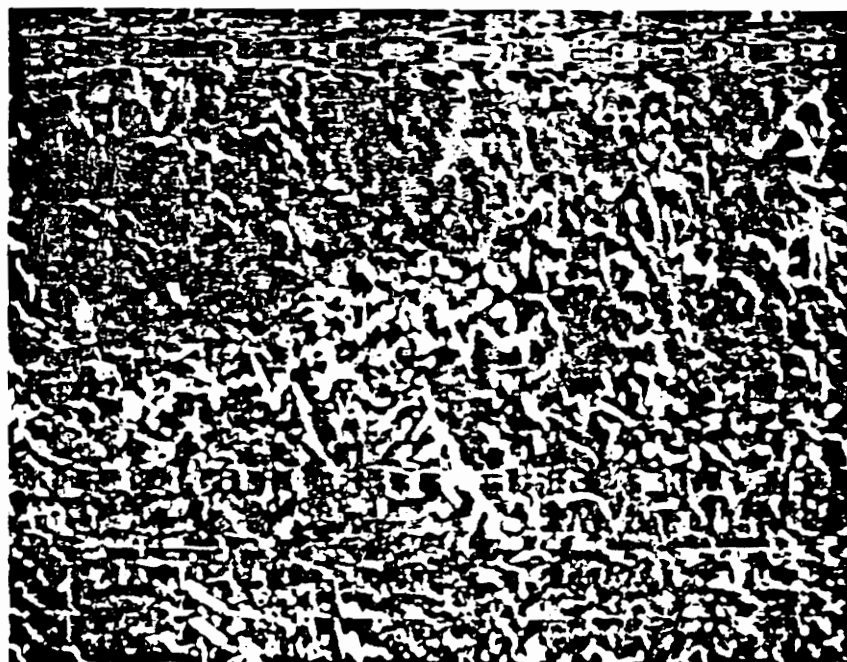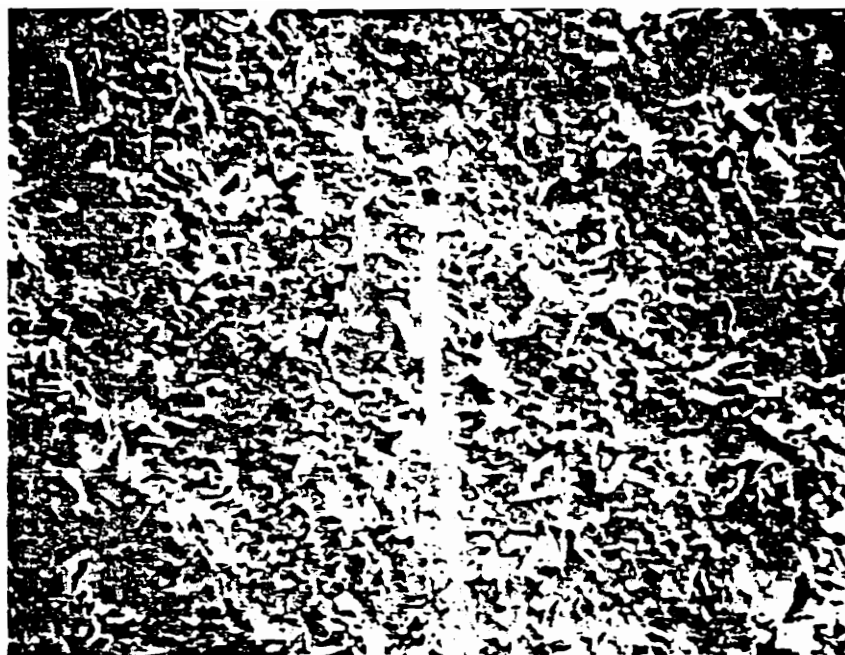
Figure 6. SEM micrographs of dielectric pastes A 4877

(K = 10) top, and A 4878 (K = 20) bottom (X2000)
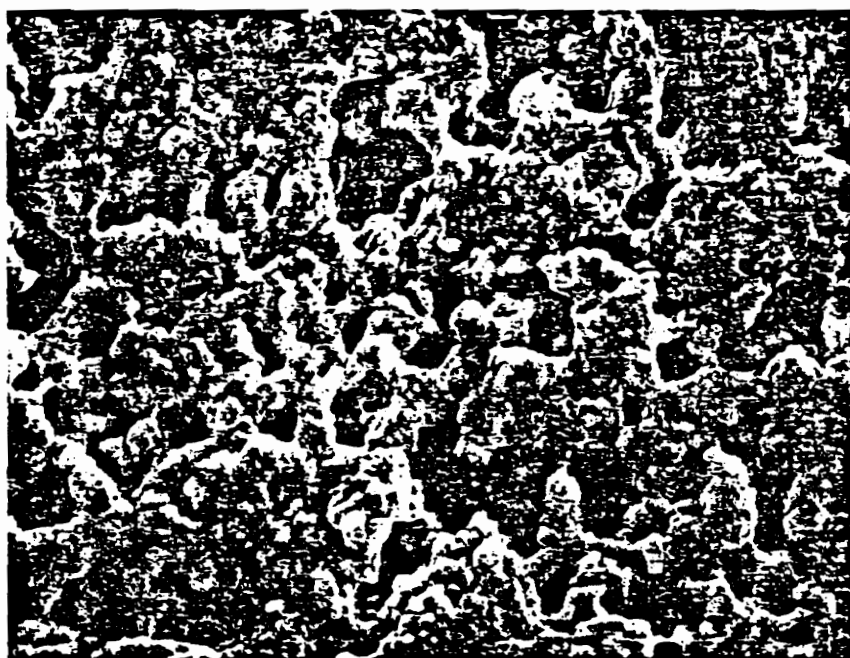
Figure 7.   SEM micrograph of dielectric paste A 4842

(K = 50) X5000

Measurement and results   24
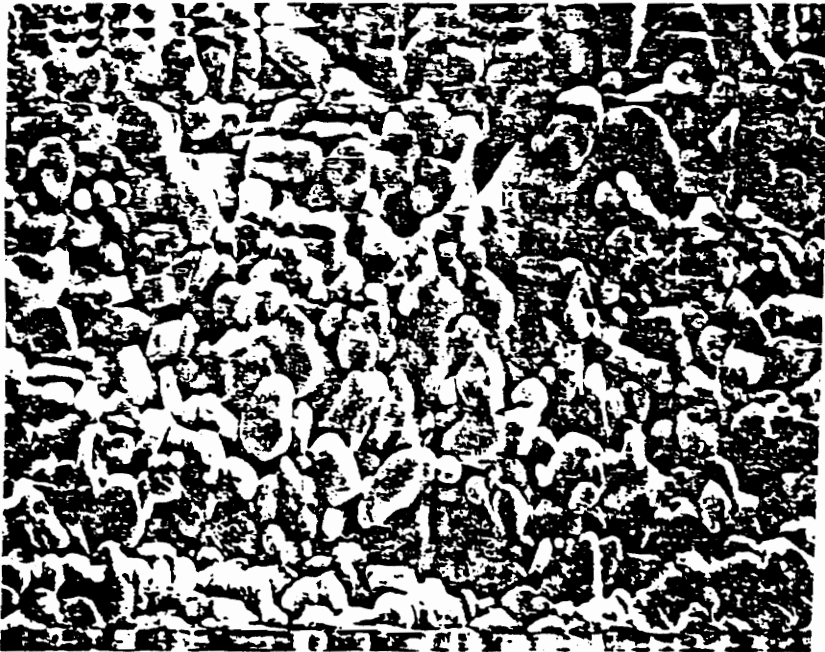
Figure 8.   SEM micrograph of dielectric paste A 4879

(K = 100) X2000

Measurement and results   25
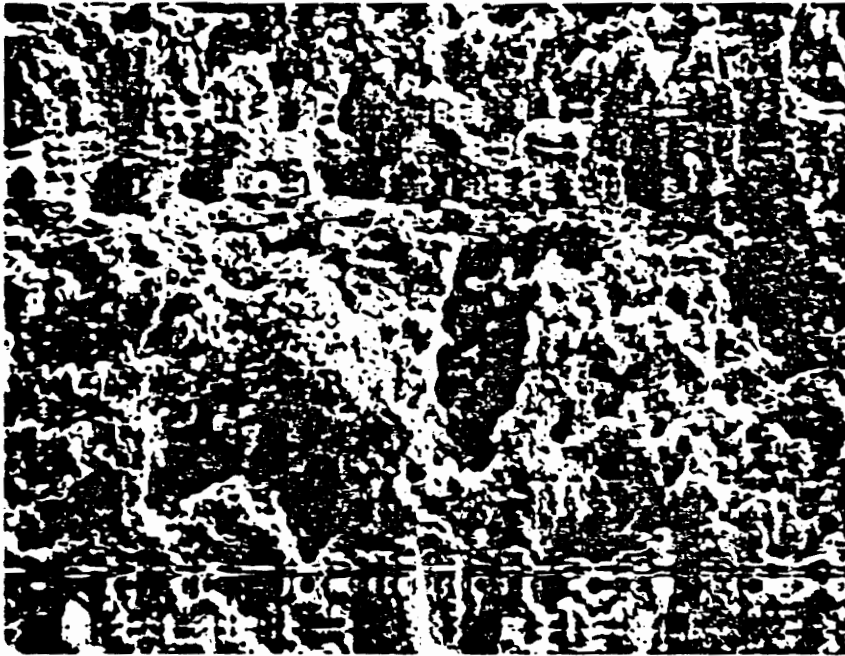
Figure 9.   SEM micrograph of dielectric paste A 4880

         (K = 300) X2000

Measurement and results

Figure 10.   SEM micrograph of dielectric paste A 4881

(K = 1000) X2000

Measurement and results   27

4.1.2 K=1000 dielectric paste

The dielectric layer under SEM examination showed needle like structures, especially at the edges of the sample. An investigation was carried out to identify the main constituent of the needle-shaped elements. EDAX analysis showed these elements to be predominantly rich in Pb, but there was also some presence of titanium. This is an example of "bleed out" [13]. It is believed that "glass bleedout" is generally more pronounced as the number of firing steps increases. Our samples were fired a total of seven times. Glass bleedout in this particular sample is from the dielectric layers as well as the Pd/Ag conductor layer. A possible explanation for this bleedout could be that the glass binder used in this paste has a greater tendency toward reduction i.e. from lead-oxide to lead.

4.1.3 Electron spectroscopy for chemical analysis (ESCA)

A substantial proportion of samples containing dielectric pastes A 4880 and A 4881 were frequently shorted. ESCA analysis was performed to confirm whether silver migration had taken place. The presence of silver in the high-K capacitor is clearly seen in Figure 15.
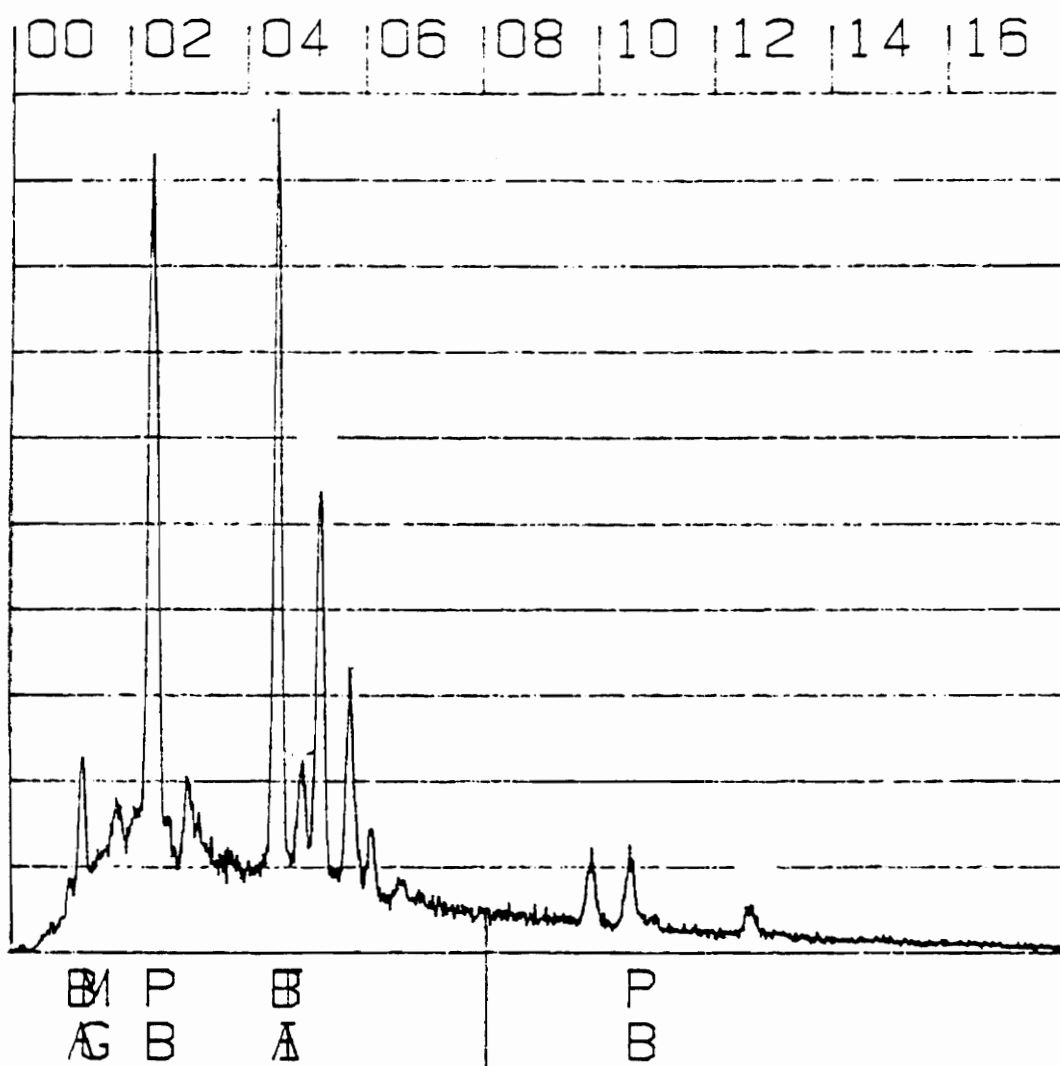
Figure 11.   EDAX analysis of K = 100 dielectric

Measurement and results
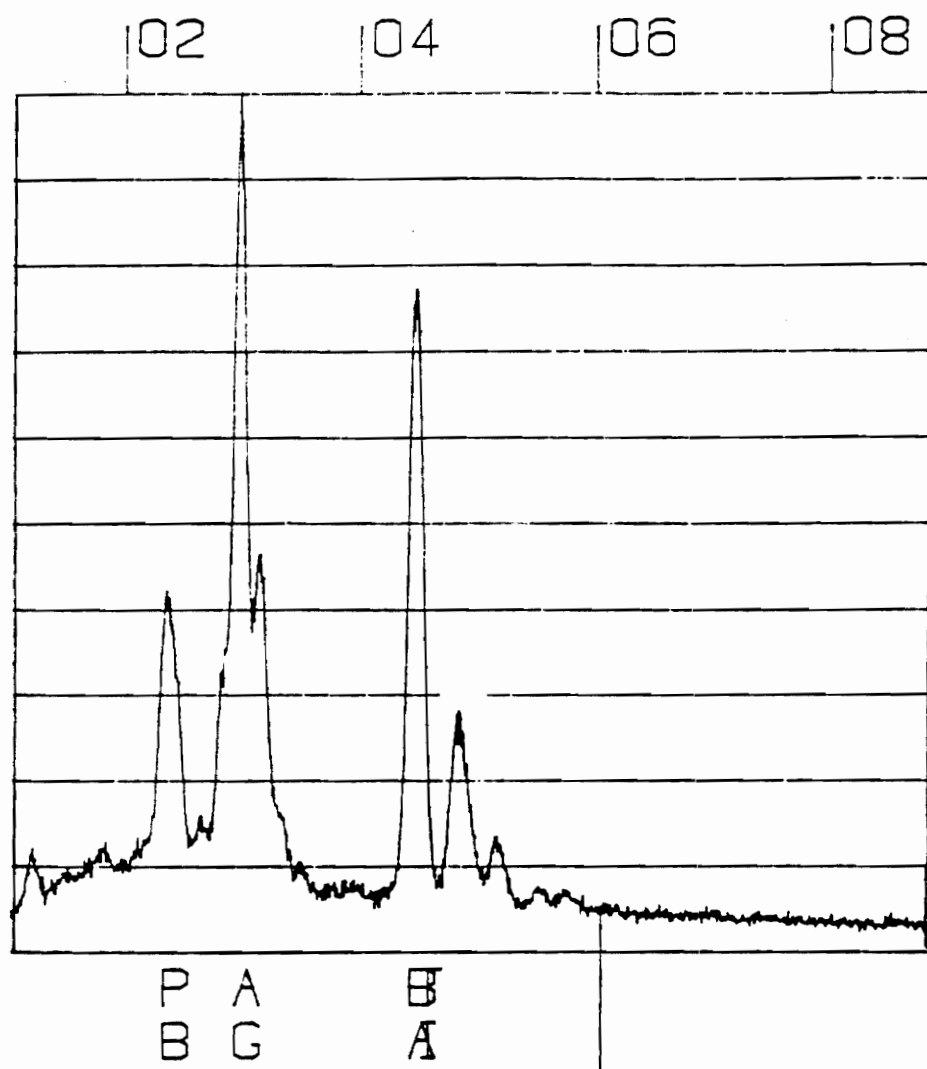
Figure 12. EDAX analysis of K = 300 dielectric

Measurement and results
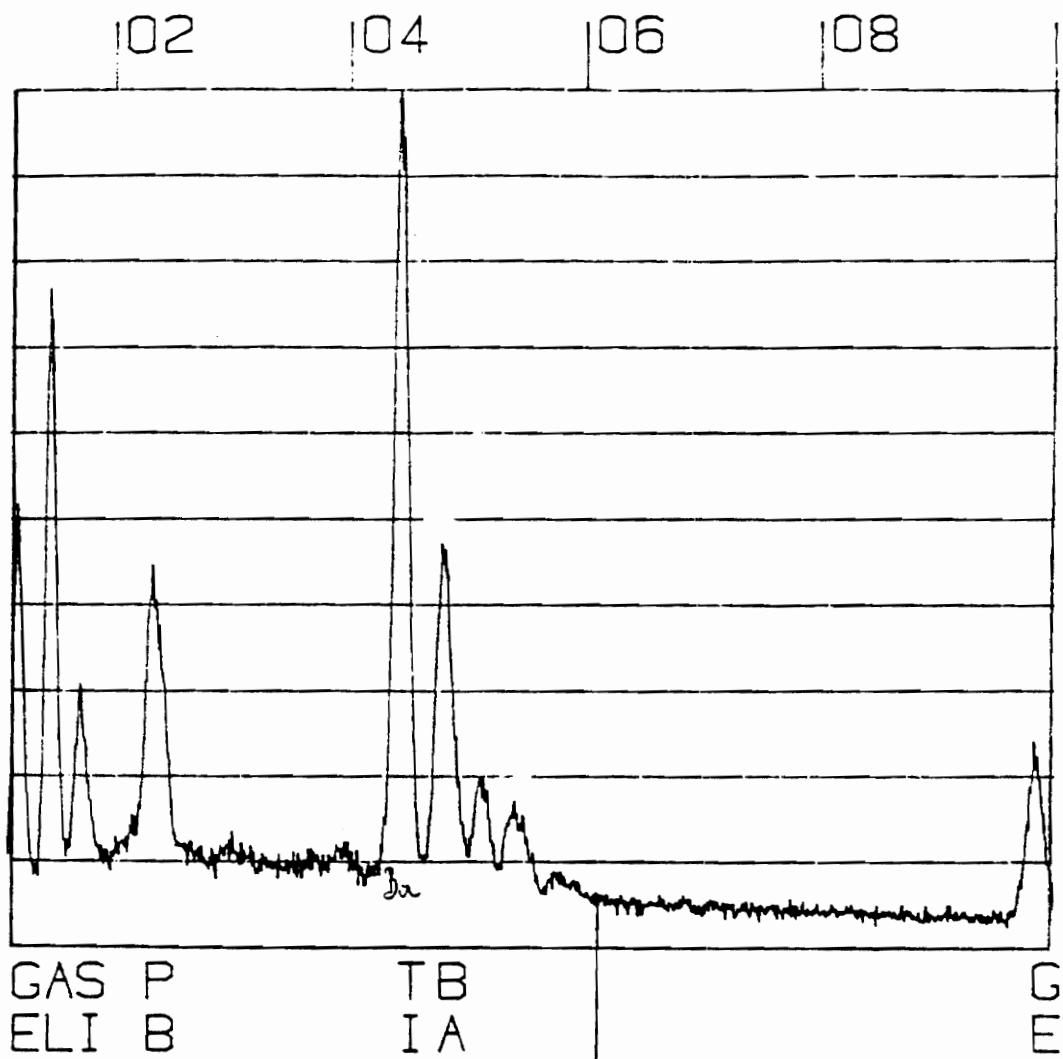
Figure 13.   EDAX analysis of K = 1000 dielectric

Measurement and results   31
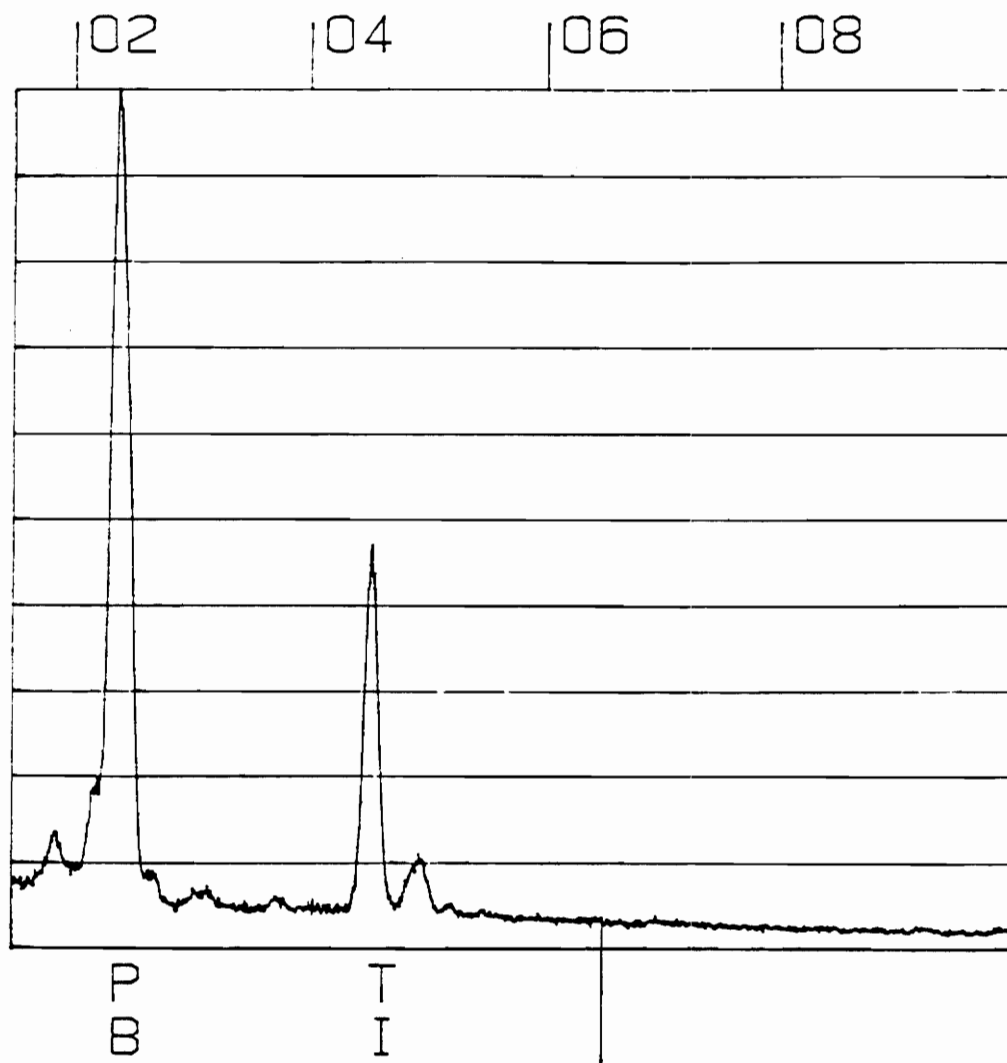
Figure 14.   EDAX analysis of needle-shaped elements

Measurement and results
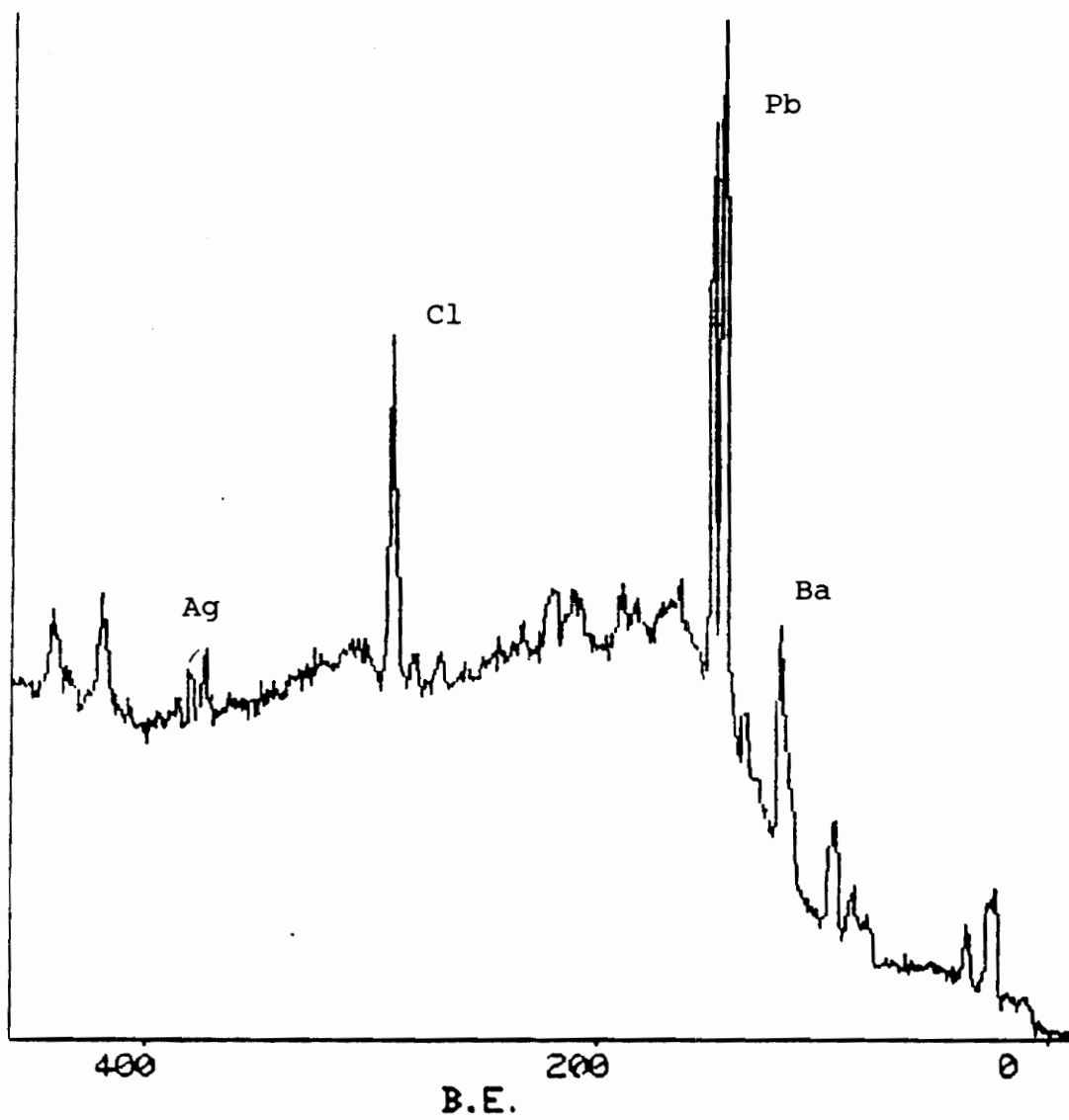
Figure 15.   ESCA of K = 300 dielectric

Measurement and results   33

4.2 Dielectric thickness

The thickness of the dielectric layer must be determined so as to calculate the dielectric constant since the capacitance, C, is given by:

$$C = 0.225 \ K \ A \ / \ t \qquad\qquad 4.2.1$$

where

C = capacitance value in pF

K = dielectric constant of the material

A = plate area in inches^2

t = thickness of dielectric in inches

From this relation a formula for determining the dielectric constant K is:

$$K = C \ t \ / \ 0.225 \ A \qquad\qquad 4.2.2$$

The capacitance was measured using an HP 4192 A Impedance Analyzer at 1 KHz.

Two methods were used for measuring print thickness, the scanning electron microscope, and the profilometer [14]. The profilometer, basically consists of a fine stylus connected to a piezoelectric crystal which generates an electronic signal proportional to the thickness. The stylus

was first used to traverse the sample containing only the bottom electrode. After the dielectric layers were printed and fired over the conductor layer, the structure was again traversed by this stylus. The difference between the two measurements yielded the dielectric thickness. To measure thickness via an SEM, it was necessary to cross-section the sample. The dielectric and the conductor layers can be clearly seen from the resulting photograph. A ruler can then be used to measure the thickness from the photographs.

The SEM has the advantage of being fast and simple, although more expensive. When measuring thickness using a profilometer, the samples do not have to be cross-sectioned. The results obtained by each method were in close agreement. However, one must remember that SEM focuses on a very small spot on the sample. Figure 16 illustrates examples of the thickness measurement techniques. The calculated dielectric constants and the thickness of the dielectrics are given in Table 5.

4.3 Electrical measurements

The capacitance, dissipation factor and conductance measurements against frequency were made using HP 4192 A LF Impedance Analyzer. A Tenney Jr. temperature chamber, and a copper box with Omega temperature controller were used for
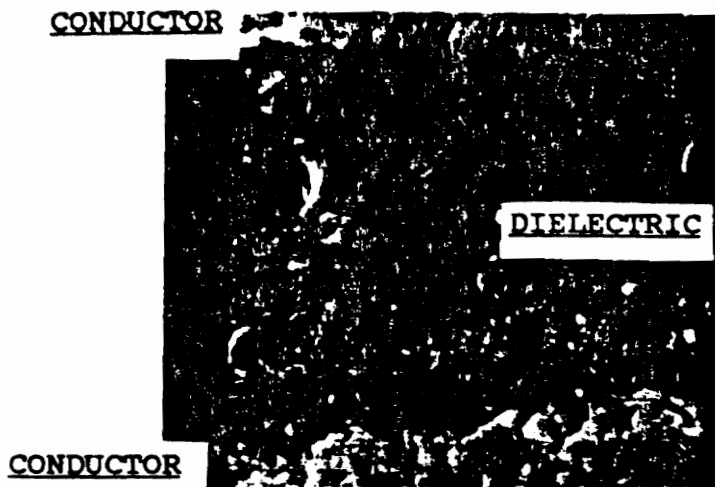
Scale: 100 microns
Scan speed: 25 mm/s
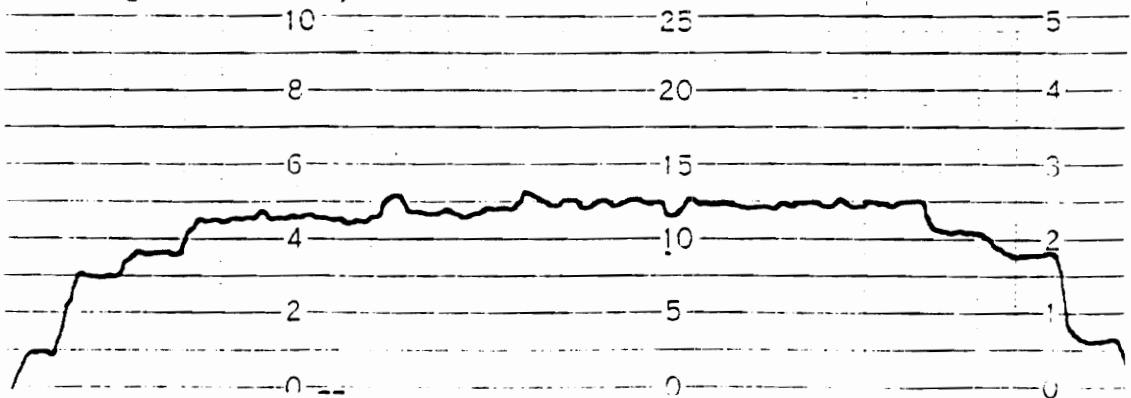
Figure 16.   Measurement of dielectric thickness
             SEM cross-section of capacitor (top), and
             profilometer reading (bottom)

Measurement and results   36

TABLE 5.   Thickness of the dielectrics and their

dielectric constants

.

Dielectric Paste	Thickness mils	Measured Dielectric Constant K	Quoted* Dielectric Constant K
A 4877	1.650	10.84	10
A 4878	0.985	15.97	20
A 4842	1.024	34.77	50
A 4879	1.103	86.13	100
A 4880	1.261	345.39	300
A 4881	1.182	698.12	1000

* Quoted by Engelhard Industries

heating the devices. A Keithley Model 480 log-ammeter, and
a Keithley 26000 picoammeter were used to measure electric
currents.

4.3.1 Insulation resistance

An HP 4329 A instrument was used to measure the
insulation resistance of the capacitors at a test voltage of
10 volts DC, after a test time of one minute. The results
are shown in Table 1.

4.3.2 Dissipation factor

The dissipation factor (DF) is calculated from the
ratio of the imaginary to the real component of the specimen
impedance (with alternating voltages the charge stored on a
dielectric has both in-phase, or real, and out-of-phase, or
imaginary, components) [15].

$$DF = \ddot{E}''/\ddot{E}' \qquad\qquad\qquad 4.3.1$$

and,
$$\ddot{E}^* = \ddot{E}' - j\ddot{E}'' \qquad\qquad\qquad 4.3.2$$

The DF measurements were performed at 1 and 10 KHz as
shown in Table 6.

TABLE 6. Dissipation factor and capacitance of samples at 1 and 10 KHz, respectively

-

Notation	Frequency KHz	Capacitance pF	Dissipation Factor
A 4877	1 10	59.60 58.26	0.0036
A 4878	1 10	146.0 145.9	0.0005
A 4842	1 10	305.7 305.5	0.0008
A 4879	1 10	704.4 701.2	0.0021 0.0035
A 4880	1 10	2476.0 2454.2	0.0055 0.0078
A 4881	1 10	5348.3 5283.0	0.0098 0.0123

4.3.3 Dielectric constant

Dielectric constant K is the ratio between the charge stored on a geometrical configuration of electrode material at a given voltage and the charge stored on a set of identical electrodes separated by vacuum. The dielectric constant is given by:

$$\text{dielectric constant } K = \ddot{E}/\ddot{E}_O \qquad\qquad 4.3.3$$

where,

$\ddot{E}$ = permittivity of dielectric material

$\ddot{E}_O$ = permittivity of free space

Figure 17 shows the variation of dielectric constant with frequency at room temperature. Figures 18 to 22 show the variation of dielectric constant with frequency for temperatures ranging from 25°C to 125°C. The frequency range used was from 5 Hz to 10 MHz.

Reactance versus frequency and capacitance versus frequency, were measured in order to calculate the dielectric constants. It was noticed that as the frequency increased, there came a point at which the capacitance began to increase. This was attributed to the resistance and inductance effects of the leads and the electrodes at higher frequencies. The effect of resistance must be almost negligible and the effects of the inductance needs to be

DIELECTRIC CONSTANT VS LOG FREQUENCY
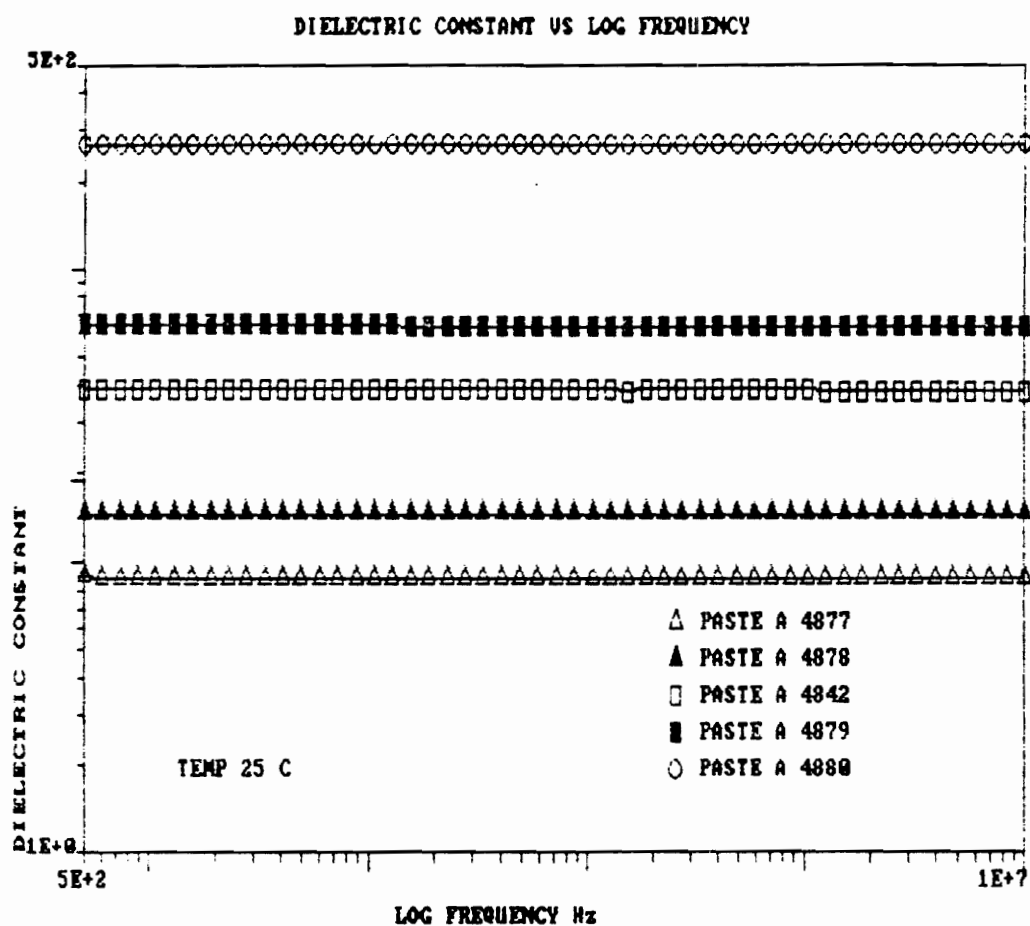
Figure 17.   Dielectric constant vs log frequency at room temperature
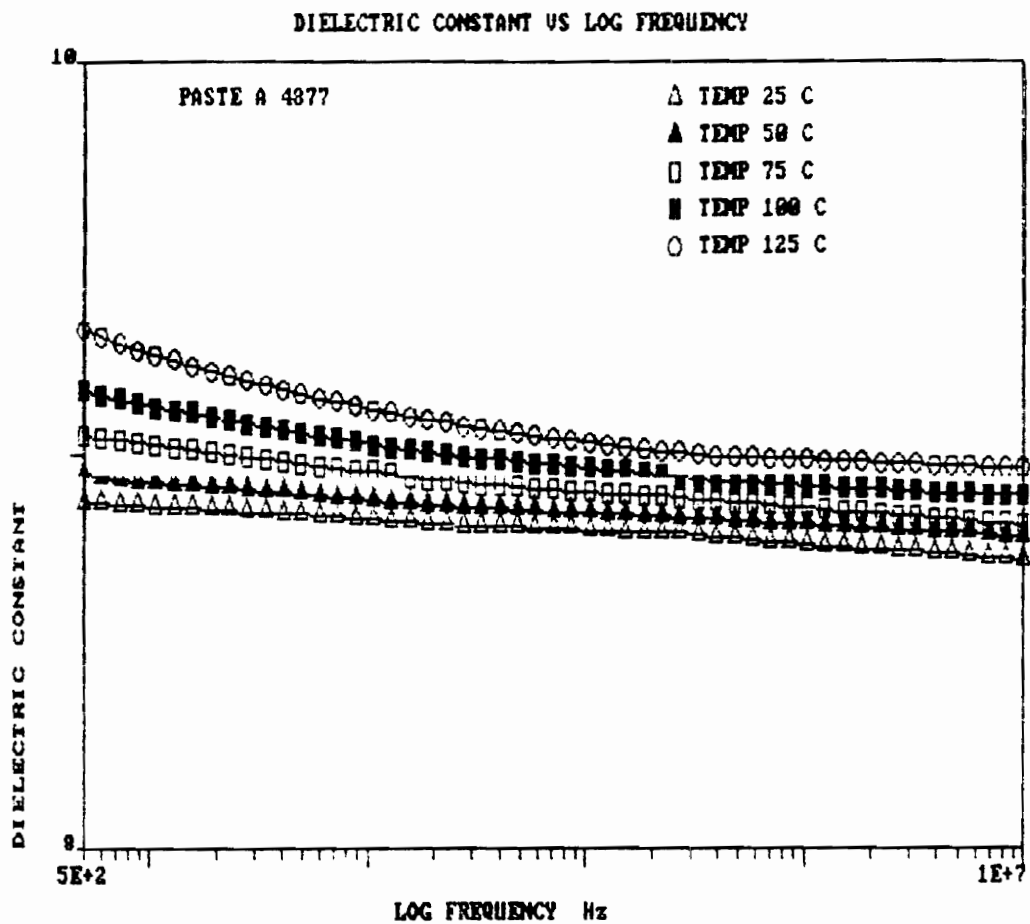
Figure 18. Dielectric constant vs log frequency for K = 10 from 25°C to 125°C

Measurement and results

DIELECTRIC CONSTANT VS LOG FREQUENCY
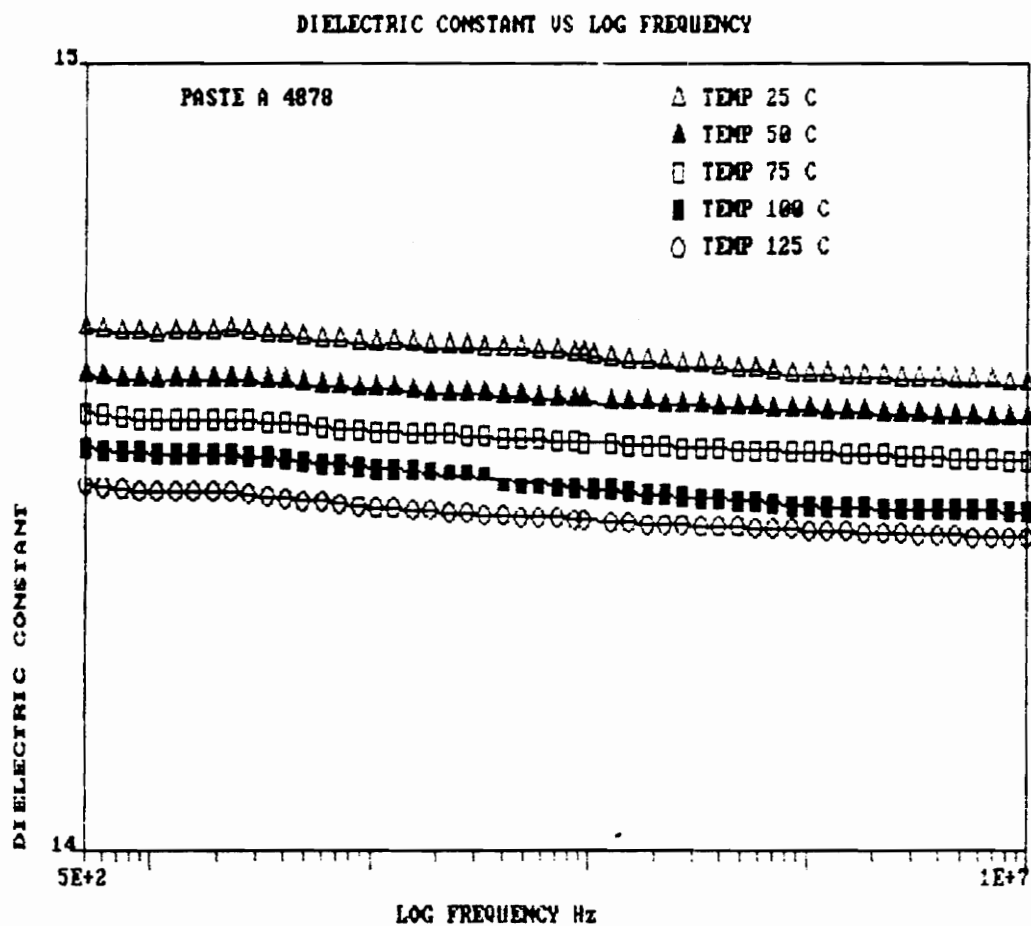
Figure 19.   Dielectric constant vs log frequency for K = 20
             from 25°C to 125°C

Measurement and results   43

DIELECTRIC CONSTANT VS LOG FREQUENCY

PASTE A 4842

△ TEMP 25 C
▲ TEMP 50 C
▢ TEMP 75 C
▮ TEMP 100 C
○ TEMP 125 C

DIELECTRIC CONSTANT
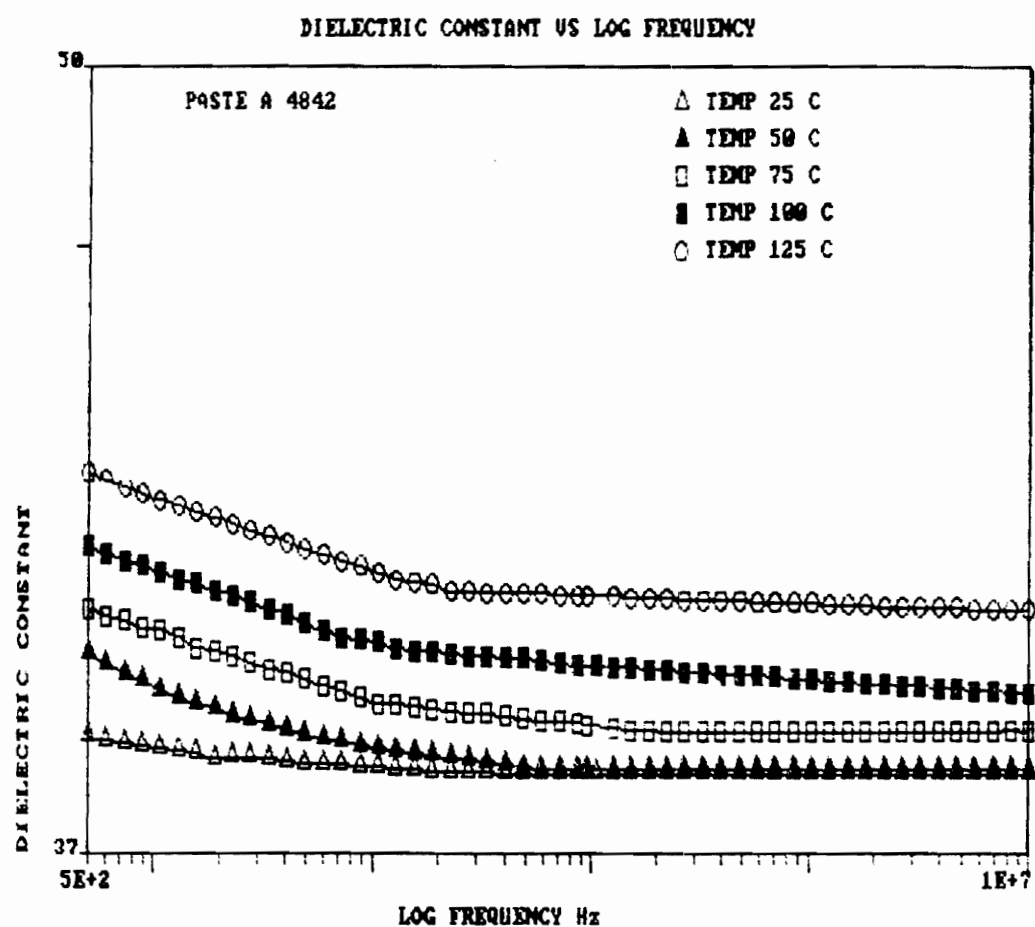
LOG FREQUENCY Hz

Figure 20. Dielectric constant vs log frequency for K = 50 from 25°C to 125°C

Measurement and results   44

DIELECTRIC CONSTANT VS LOG FREQUENCY
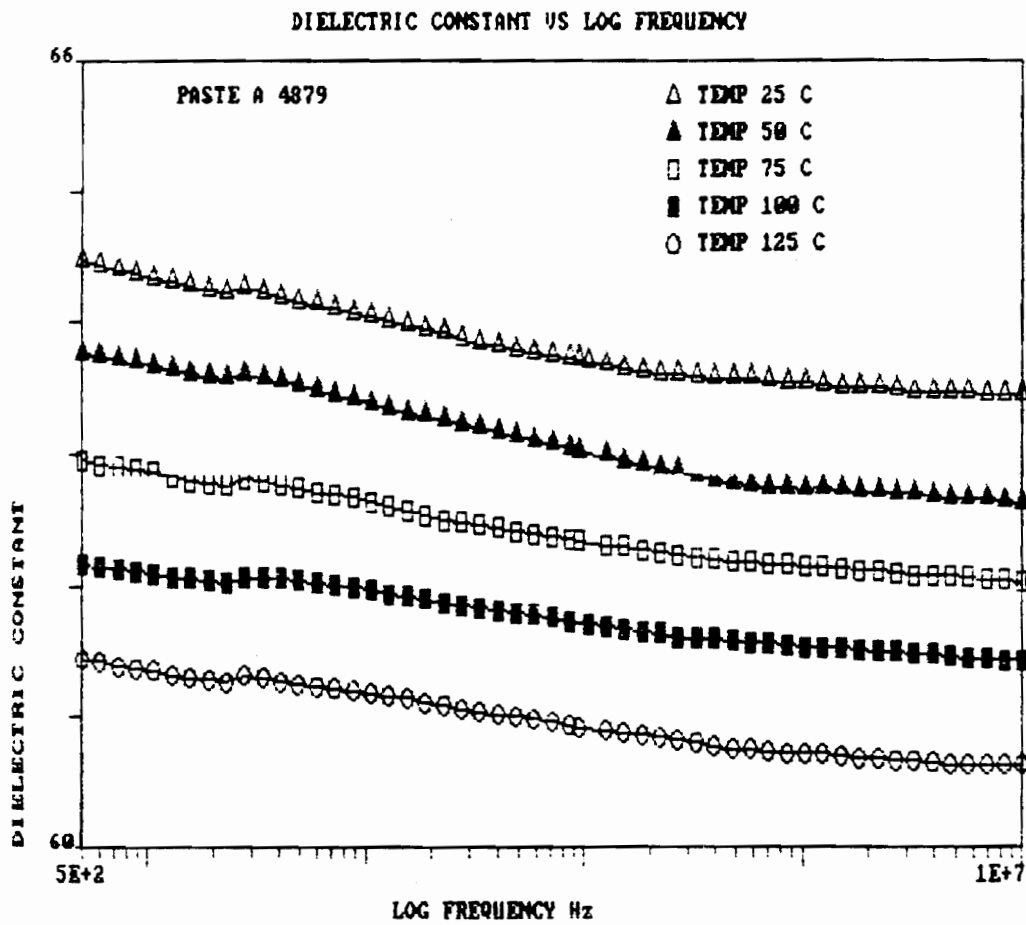
Figure 21. Dielectric constant vs log frequency for K = 100
from 25°C to 125°C

Measurement and results   45

DIELECTRIC CONSTANT VS LOG FREQUENCY
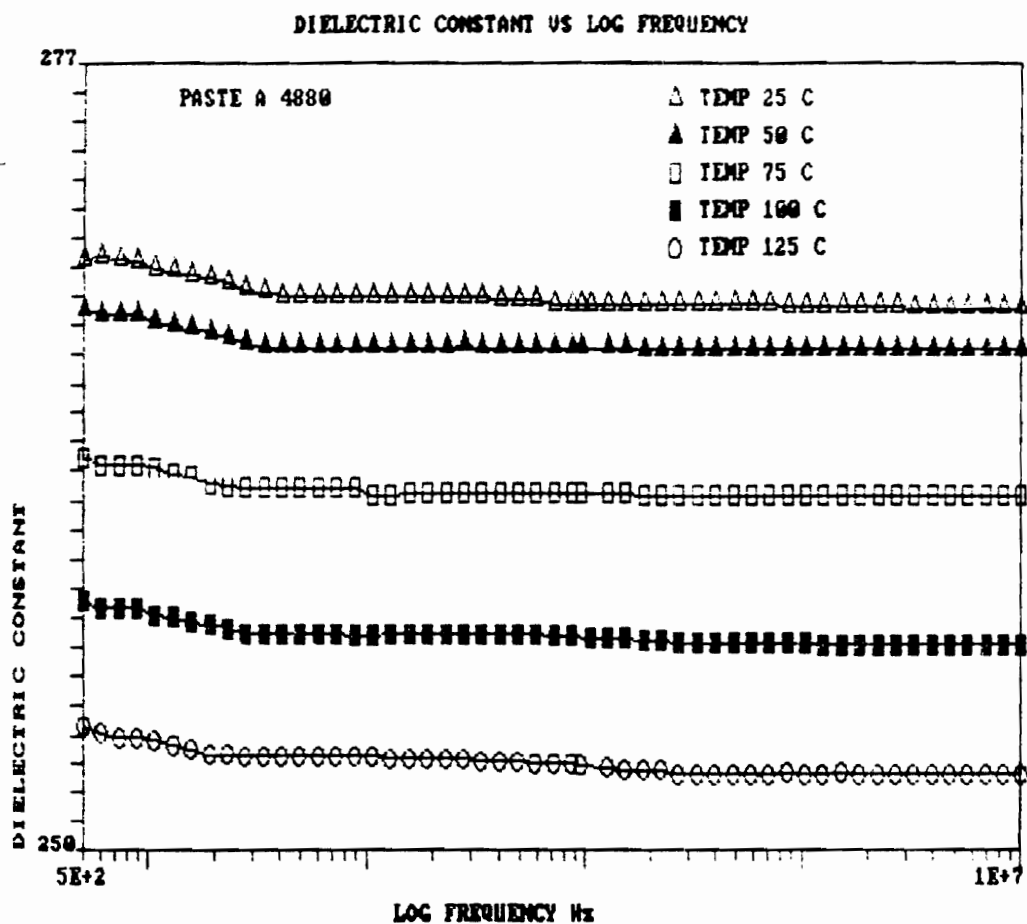
Figure 22.   Dielectric constant vs log frequency for K = 300
              from 25°C to 125°C

Measurement and results

taken into account. A method was devised to account for the capacitance. First, the reactance versus frequency measurements were recorded and then the following equation was used to determine an equivalent theoretical curve:

$$X = w\, L - 1/w\, C \qquad\qquad 4.3.4$$

where,

X = reactance of the capacitor,

L = inductance of the leads and electrodes,

C = capacitance,

w = angular frequency

    Using the value of the capacitance measured at the lowest frequency, an initial estimate was made for the value of the inductance. A curve was then constructed using the above values and compared to the actual reactance versus frequency plot. It is found that, when a good estimate is made for L, the two curves are approximately the same. At low frequencies, the curves match each other almost exactly whereas, at higher frequencies, they differ by about 2%, which is attributed to dispersion. Values of inductance are repeatedly substituted until the most appropriate one is arrived at. The correct value is then used in the following equation to calculate the actual capacitance:

$$C = \{w\, (w\, L - X)\}^{-1} \qquad\qquad 4.3.5$$

Measurement and results

Plotting the above relation, we find that the capacitance does decrease slightly with increasing frequency. The electrode inductance value of 170 nH was frequently found to be satisfactory. Then, the dielectric constant K was calculated using equation 4.2.2. The procedure was made considerably simpler by using a computer program [30].

One notices that the dielectric constant differs from the manufacturer's value for high-K capacitors. This will be discussed in chapter 5.

4.3.4 I-V measurements

Leakage currents were measured as a function of applied voltage. The stabilized currents were recorded at each voltage and temperature. Generally, the thick-film capacitors were quite unstable under temperature and voltage stress; the I-V measurement was made at a temperature and voltage of 150°C and 100 V.

Figures 23 and 24 show leakage currents for overglazed samples. As expected, the overglazed samples generally had much lower values of current.

4.3.5 Conductance vs frequency

The conductance versus frequency plots were obtained
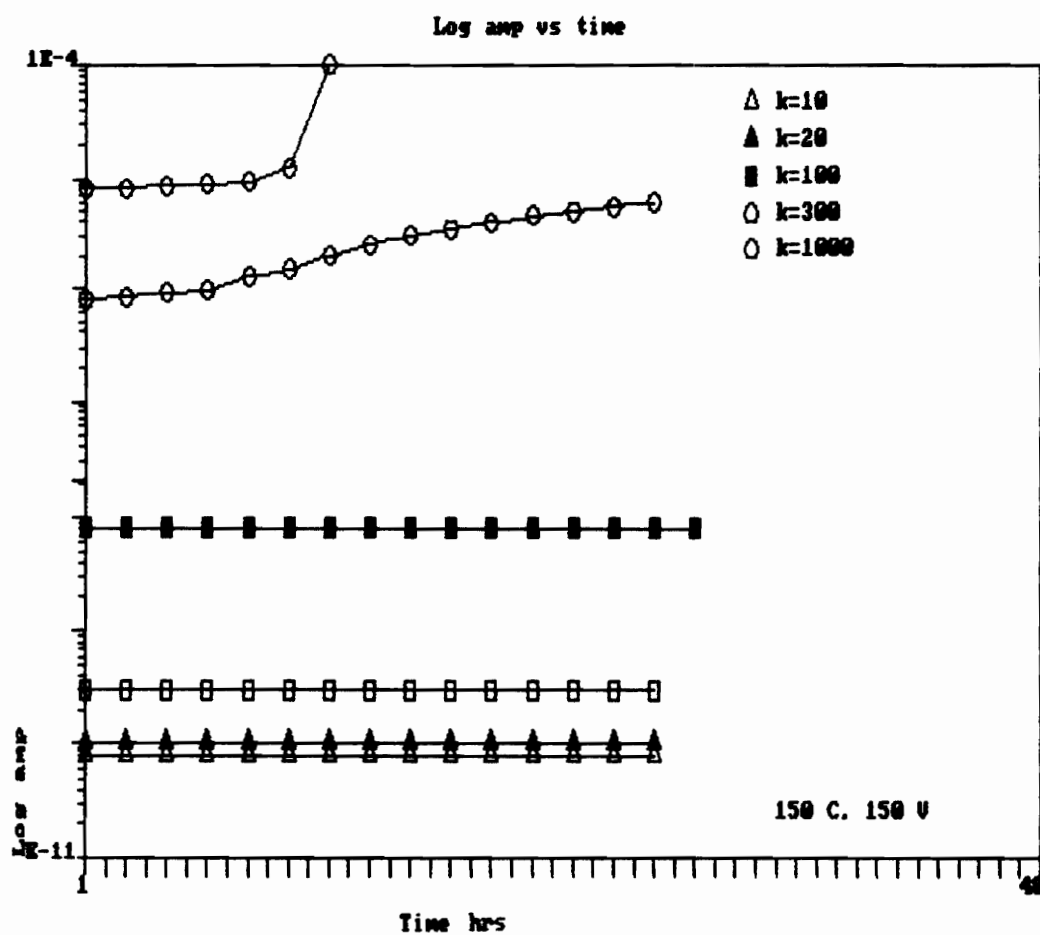
Figure 23.   Leakage current measurements of overglazed
             samples

leakage current vs time
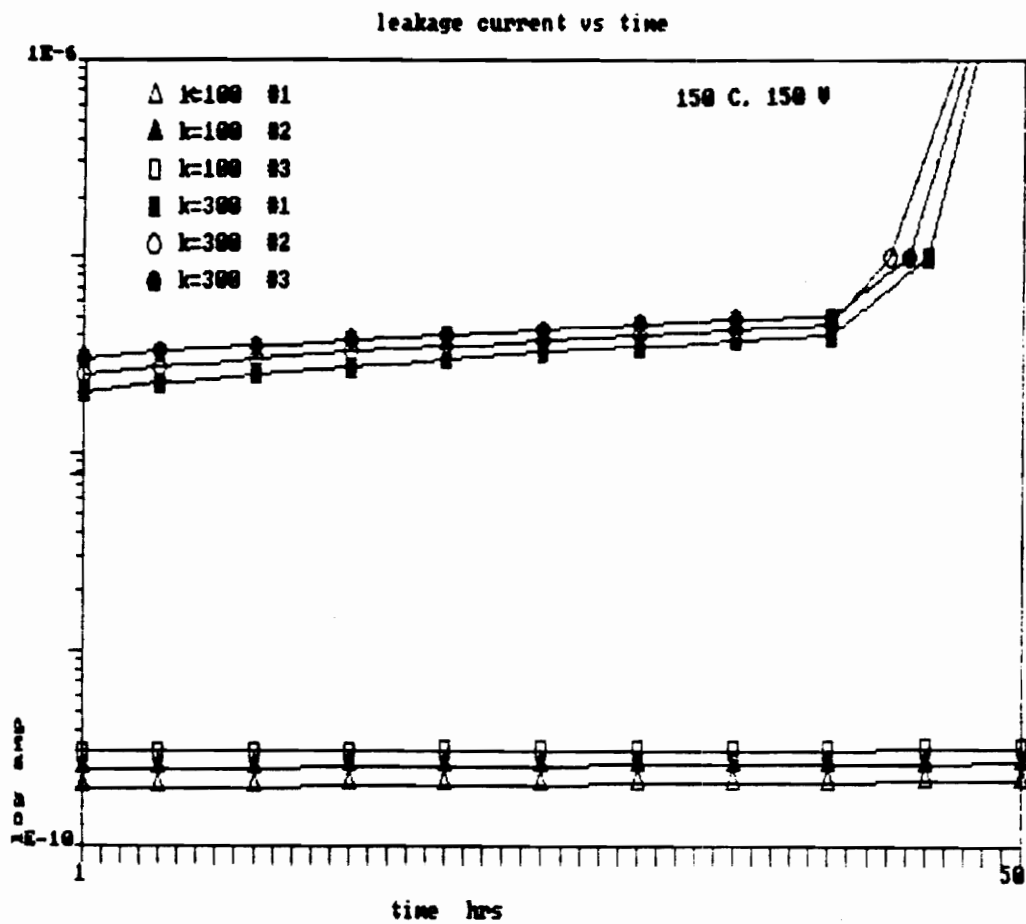
Figure 24. Leakage current measurement of K = 100 and K = 300 samples

for all the dielectric pastes as shown in Figure 25. This graph clearly indicates the lossy nature of high-K dielectric materials as compared to the low-K dielectrics.

4.4 Gain vs frequency

Gain versus frequency plots were obtained for both the RC active filter circuits. Figures 26 to 29 show the plots for the lowpass filter, with the various combinations of dielectric materials used for the fabrication of the buried capacitors. As anticipated, the circuit parameters are different for the ideal and the lossy cases. From these results one can clearly see the effect of the high-K capacitors which have very low Q's. Ideal plots for both the lowpass and bandpass filters are shown in Figures 30 and 31.

To determine the measured center frequency and quality factor (Q) of the circuit, the following items of equipment were used:

(i)   Tektronix Function Generator (with a low output impedance of 5-50 ohms),

(ii) Tektronix 60 MHz Oscilloscope,

(iii) Fluke 8012 A digital voltmeter

The frequency response was measured using the set up shown in Figure 32.

CONDUCTANCE VS FREQUENCY

capacitor with K=10
capacitor with K=20
Capacitor with K=50
capacitor with K=300
capacitor with K=1000

CONDUCTANCE X E-9 SIEMENS
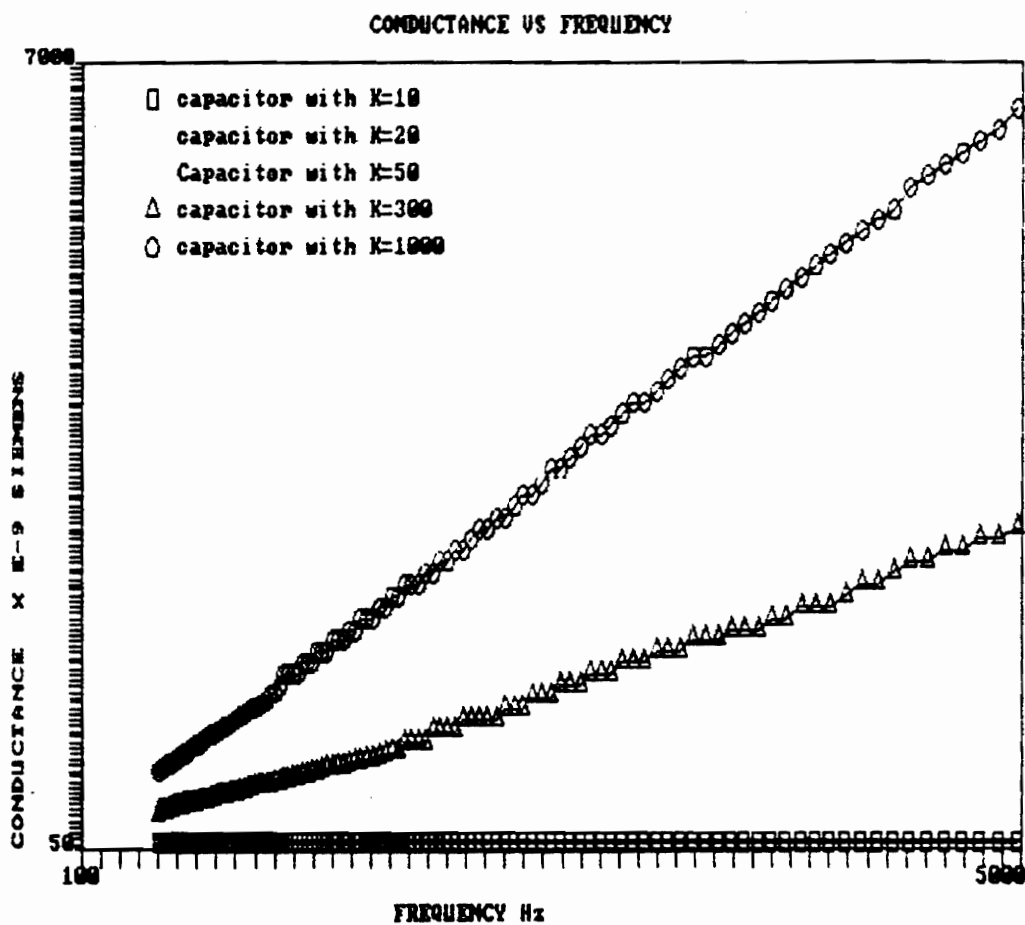
FREQUENCY Hz

Figure 25.   Conductance vs frequency plot of the dielectrics

Measurement and results   52

Center frequency   710 Hz

Q theoretical-ideal   3.24

Q measured   2.89
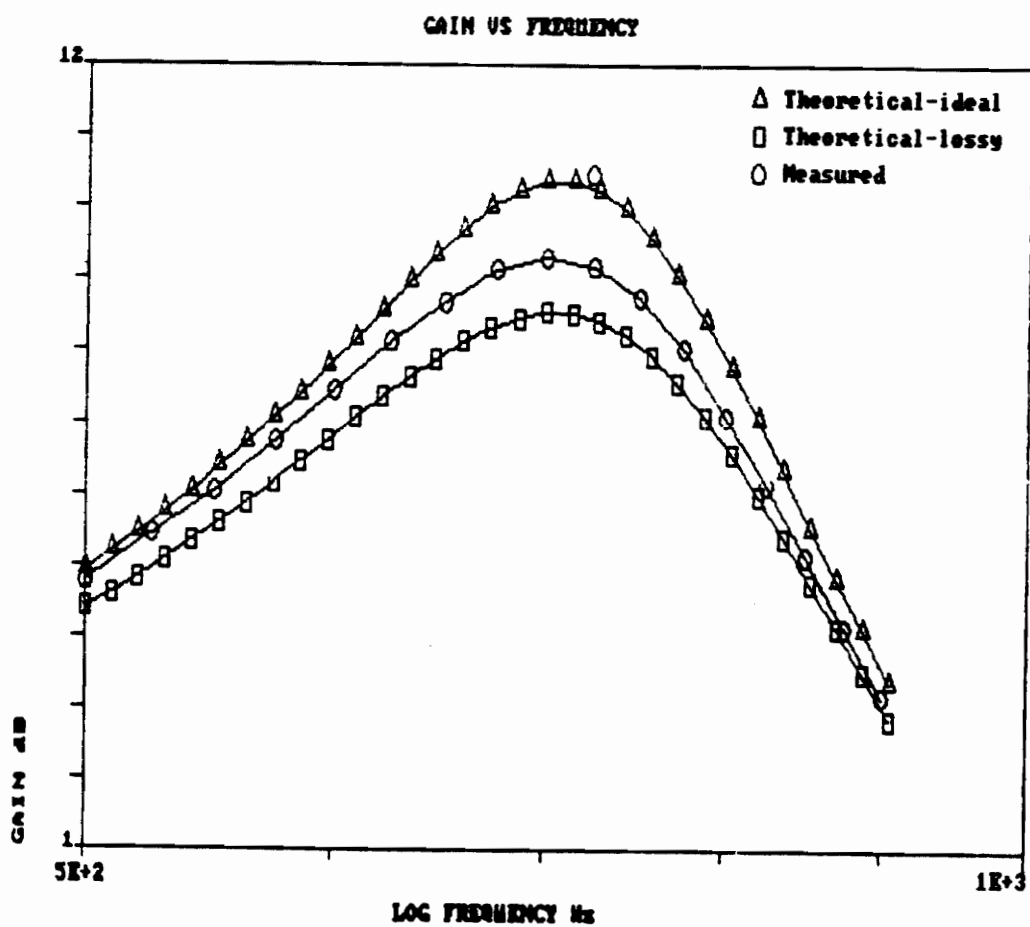
Figure 26. Gain vs log frequency for lowpass filter
           with K = 20 and K = 1000 combination for
           the two buried capacitors

Measurement and results   53

Center frequency   1075 Hz

Q theretical-ideal   5.16

Q measured   4.37
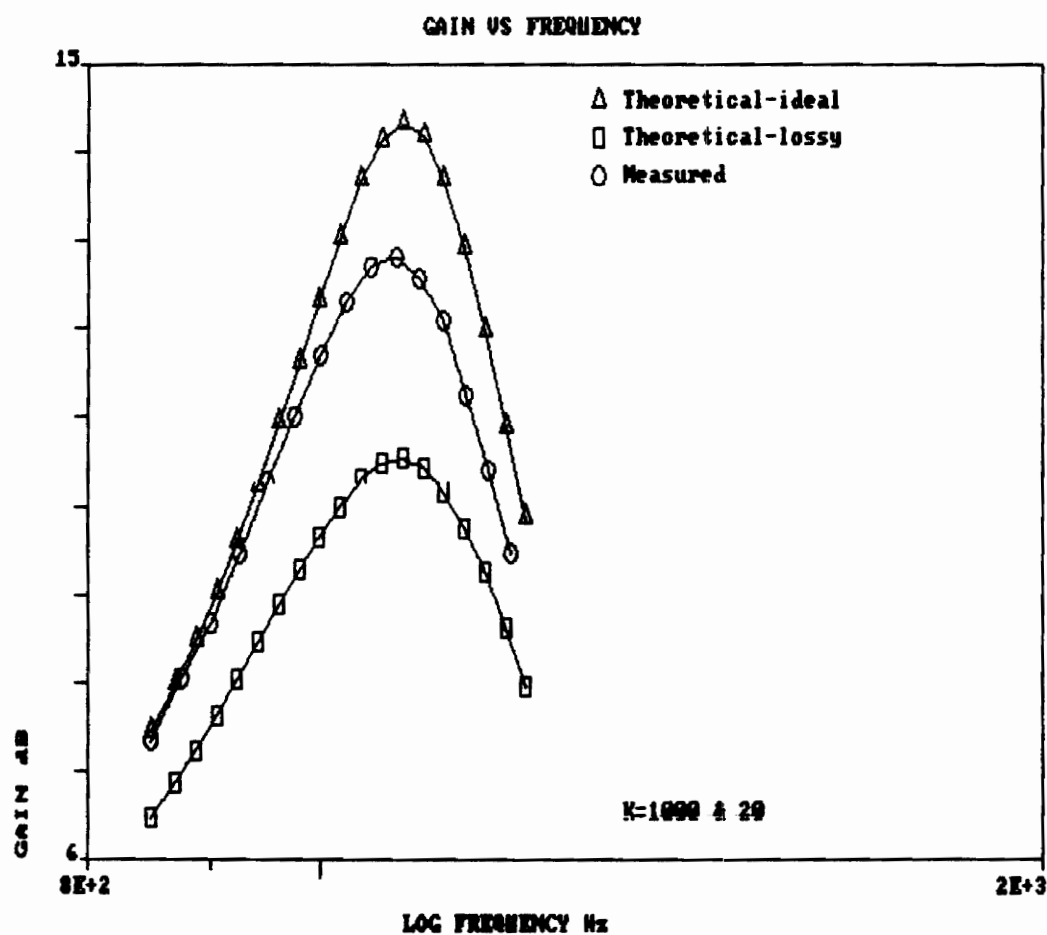
GAIN VS FREQUENCY

Figure 27.   Gain vs log frequency for lowpass filter
             with K=50 and K=1000 combination for
             the two buried capacitors

Measurement and results   54

Center frequency   1325 Hz

Q theoretical-ideal   4.05

Q measured   3.45
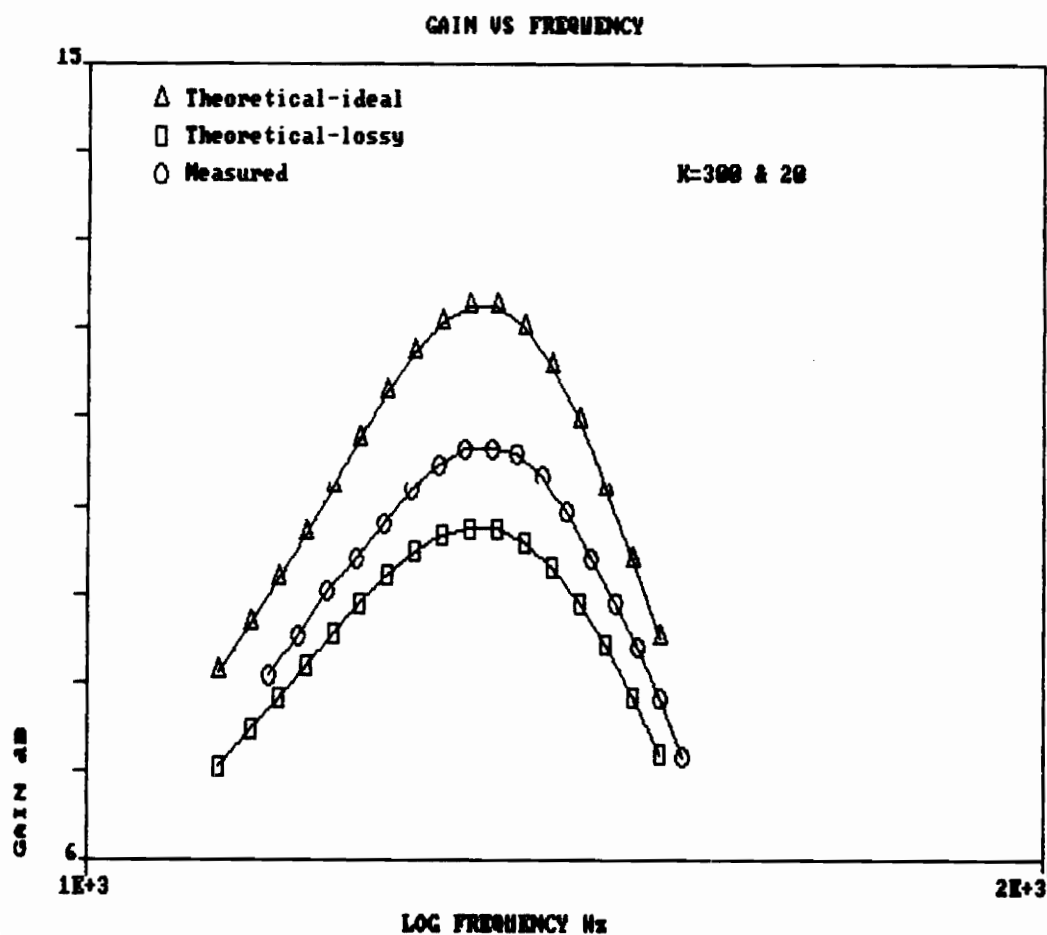
Figure 28. Gain vs log frequency for lowpass filter

        with K=20 and K=300 combination for

        the buried capacitors

Measurement and results   55

Center frequency   885 Hz

Q theoretical-ideal   2.76

Q measured   2.60
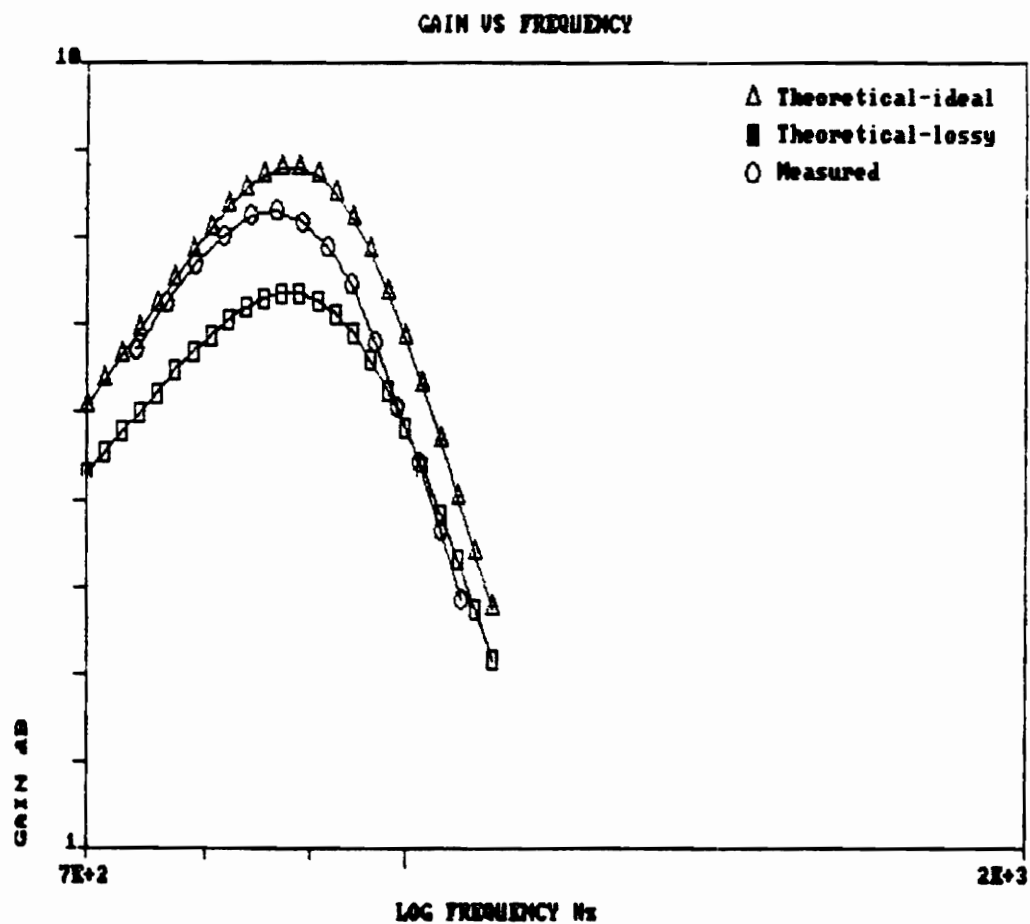
Figure 29. Gain vs log frequency for lowpass filter
            with K=50 and K=300 combination for
            the buried capacitors

Measurement and results   56
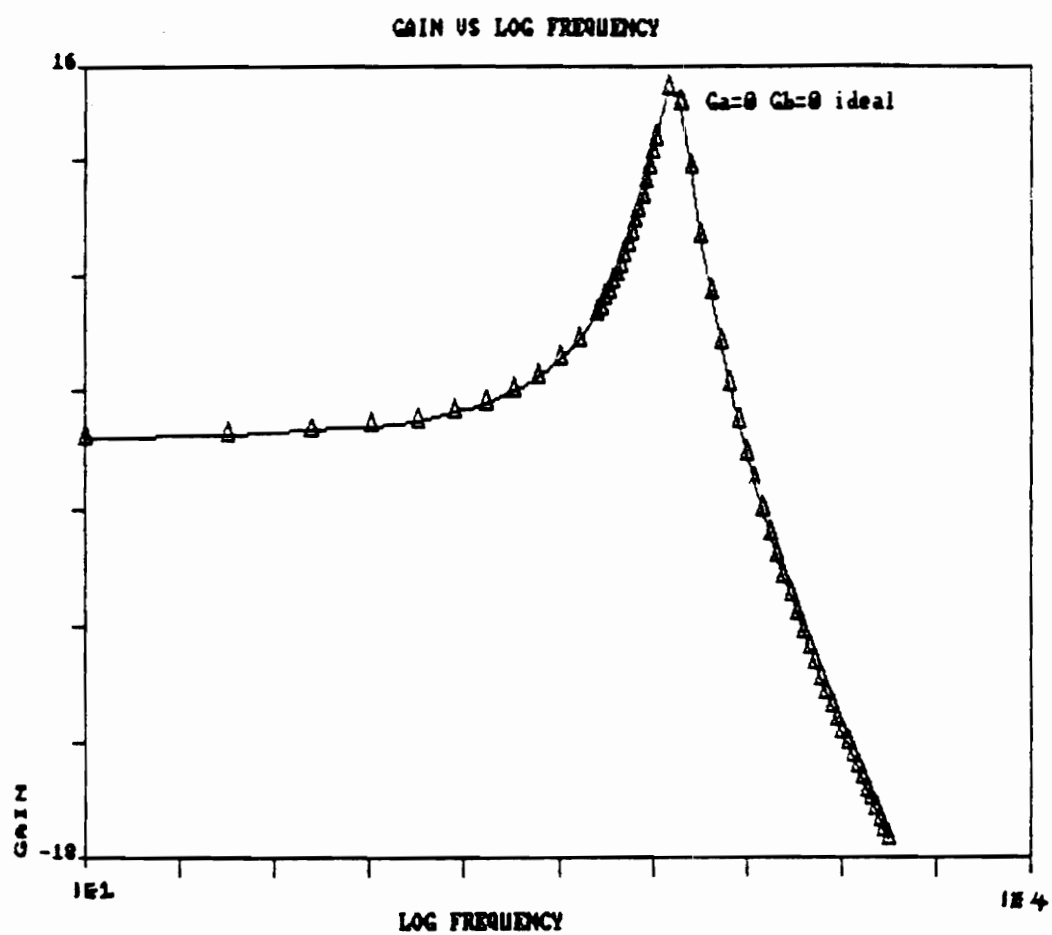
Figure 30.   Theoretical-ideal Gain vs log frequency plot for
            lowpass RC active filter

Measurement and results   57

gain vs frequency

△ bandpass filter

gain db

1E+0   1E+4

Log frequency hz
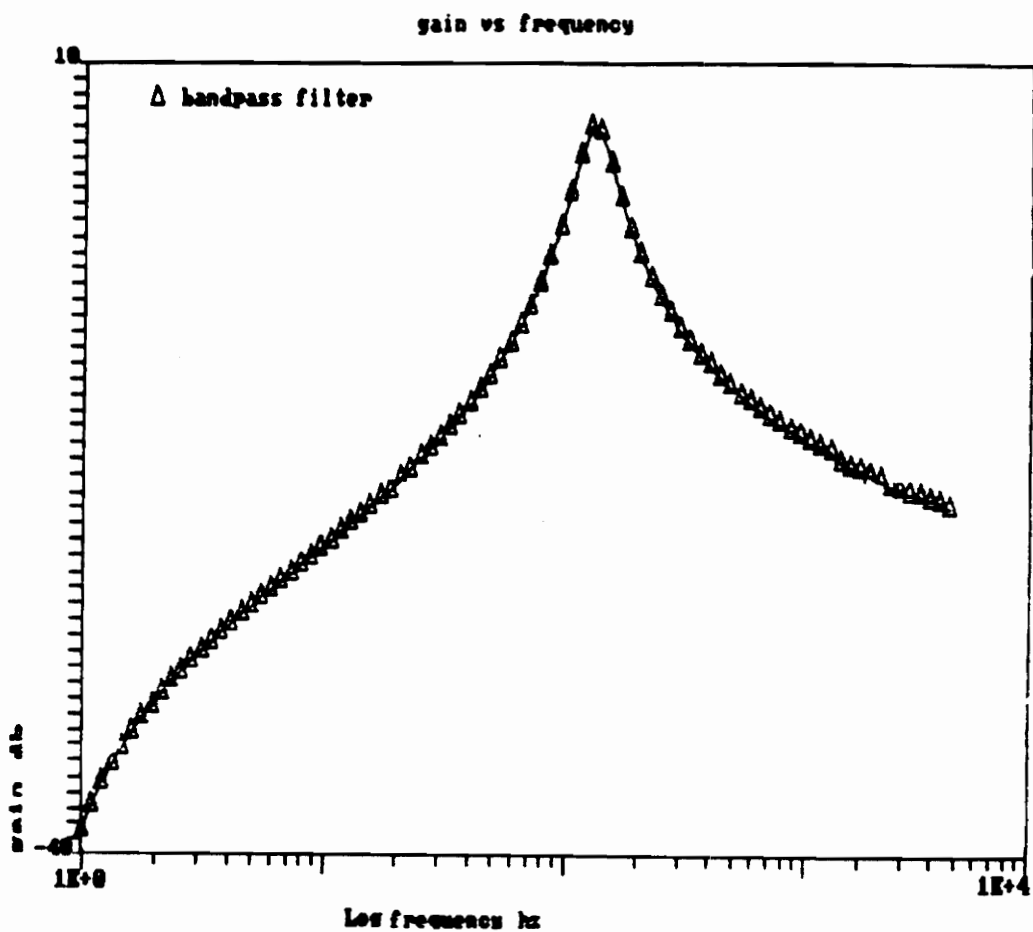
Figure 31. Theoretical-ideal Gain vs frequency plot for
            bandpass RC active filter

Measurement and results   58

oscilloscope. The power supply was set at +12, 0, -12 V DC for LF 351 op-amp. The circuit was fed with a sinusoidal 1 volt peak-to-peak input signal, with the frequency adjustable over the frequency range. At the center frequency, the response passes through a 90° phase shift which corresponds to a circular Lissajous pattern (see Figure 32). Readings of V_{out} were taken at intervals of 250 Hz. These were later converted into dB values to make plots of gain versus frequency. Also, the output waveform on the oscilloscope was monitored at all times to avoid recording voltmeter readings of saturated or noisy waveforms. The analysis and equations used to obtain theoretical-ideal and theoretical-lossy curves are presented in Chapter 5.

Test arrangement
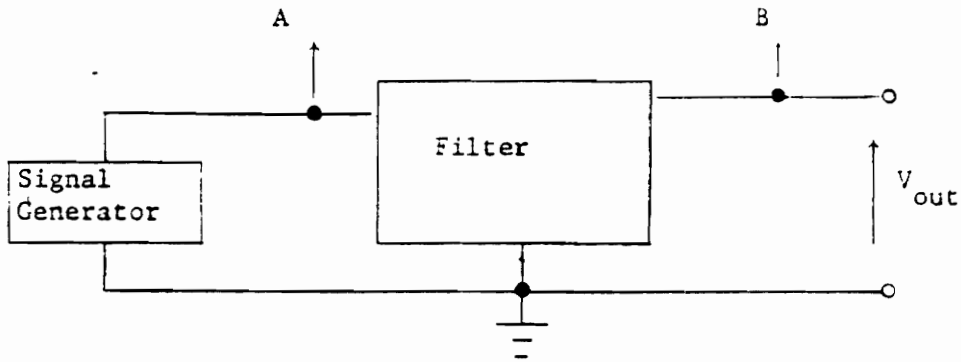
* Connect A, B to the X, Y plates of an oscilloscope
* Adjust the frequency to give the appropriate pattern from those illustrated below.

Lissajous figures

$\varphi = 0$ or $360°$

$\phi = 45°$ or $315°$

$\phi = 90°$ or $270°$

$\phi = 135°$ or $225°$

$\varphi = 180°$
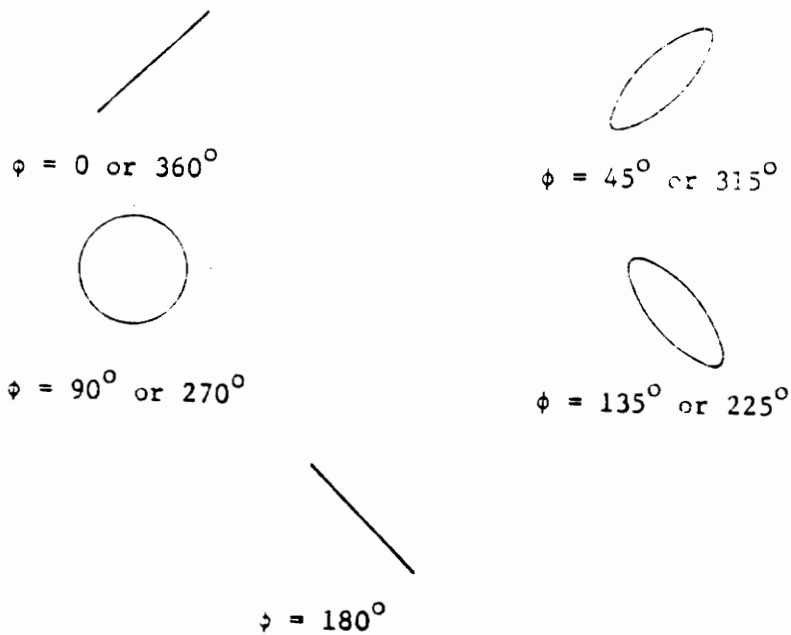
Figure 32.   Measurement schematic and examples of Lissajous patterns

CHAPTER 5. DISCUSSION

5.1 Thick-film capacitors

5.1.1 Thickness variations

It was noticed that thickness values seemed to differ from substrate to substrate. A number of factors are involved when measuring thickness. The most important parameter which affects thickness is that of screen mesh size. The lower mesh sizes give greater thickness, since the spaces between the wires are larger. One has to consider the effect of substrate camber when the profilometer is used to measure the dielectric thickness. The emulsion thickness also plays an important part in the final uniformity of the printed material. Table 7 includes a list of printing factors that affect thickness.

5.1.2 Dielectric / Conductor interactions

Complex interactions between the conductor and dielectric often occur as a result of the dynamic conditions during firing [17]. The compatibility of these dielectrics with conductors, coupled with good environmental stability to assure high reliability, is of prime importance. The microstructural development of a thick-film dielectric can significantly affect its performance characteristics. If

Conclusions and recommendations   61

TABLE 7. Printing factors that affect the thickness
of the dielectric layers

```
substrate camber

emulsion thickness

squeegee angle of attack

breakaway distance

screen mesh size

viscosity
```

CAMBER.

The amount of overall warpage present in a substrate.

BREAKAWAY.

The distance between the upper surface of the surface of
of the substrate and the lower surface of the screen when
the screen is not deflected by the squeegee.

ANGLE OF ATTACK.

The angle between the squeegee face of a thick-film
printer and the plane of the screen.

EMULSION

The light-sensitive material used to coat the mesh of a
screen.

the dielectric develops full density too early in the firing sequence, as was the case with paste A 4879 (K=100), problems such as poor burnout of the organic with resultant blistering can occur.

Figure 33 shows three examples of dielectrics. Example 1 represents a fully densified microstructure while Example 3 represents incomplete sintering of the dielectric. The porosity of the dielectrics increases from Example 1 (which contains a few isolated pores) to Example 3 (which is characterized by interconnected pores). Example 2 has intermediate porosity. From the SEM micrographs shown in Figure 9, it can be seen that Example 3 closely matches the high-K dielectrics used to fabricate capacitors in this research project. A thin interaction zone is depicted between the dielectric and the conductor layers. The formation of the interaction zone with a fully dense microstructure illustrates chemical compatibility between the dielectric and conductor. The performance properties corresponding to these microstructures (Examples 1 through 3) are presented in the same figure. The excellent electrical performance is observed for regions 1 and 2 while serious deficiencies are observed in region 3 where incomplete glass sintering has produced a dielectric with an interconnected pore structure (Example 3). This is the main reason that the high-K dielectrics, especially A 4881 (K=1000), have performed so poorly.
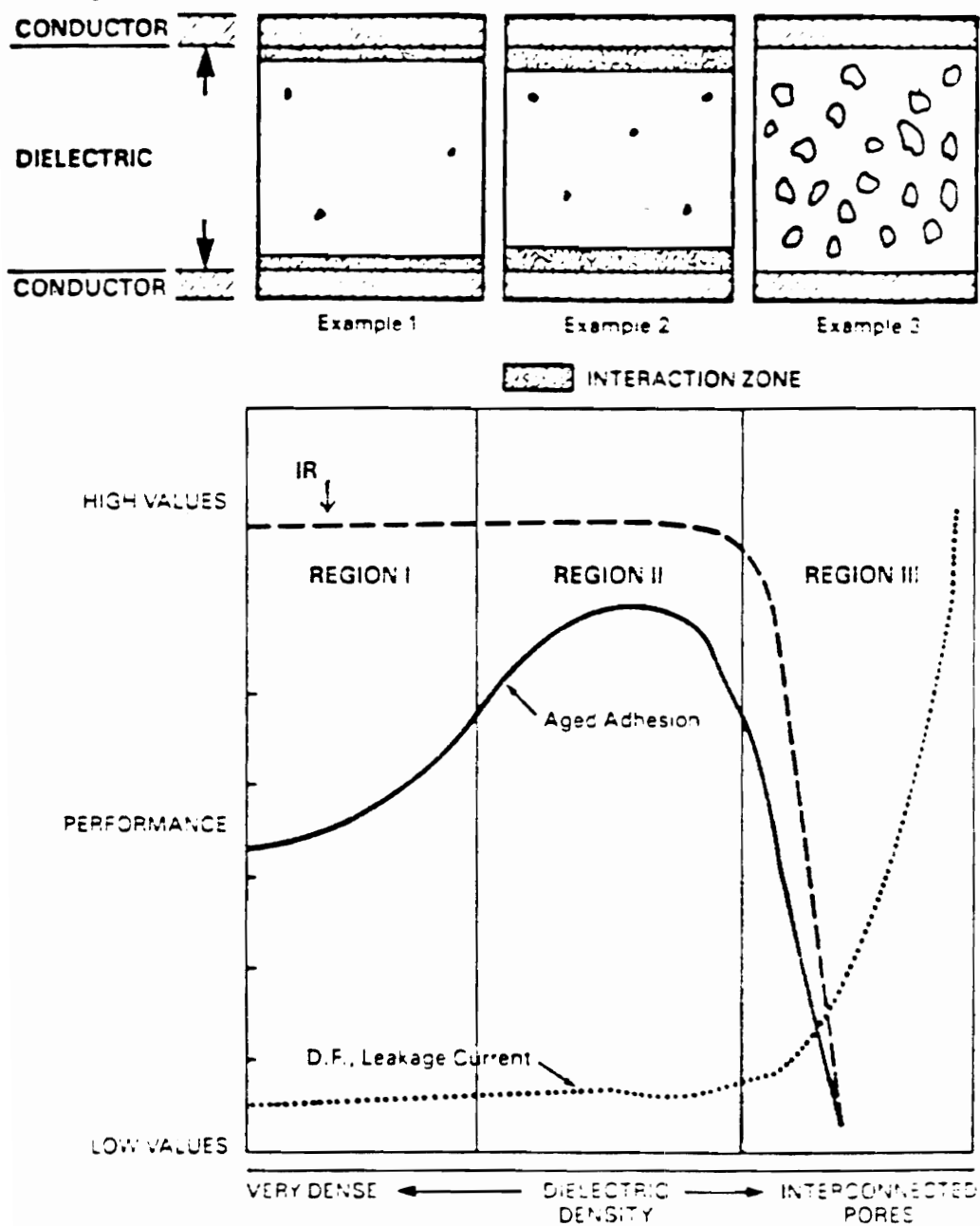
Figure 33. Performance vs microstructure

Discussion

5.1.3 Overglaze

The dielectric constant values for the overglazed samples were slightly higher than for the unglazed samples. This is attributed to the fact that the overglazed samples underwent a greater number of firings. This had an effect in reducing the thickness of the dielectric, which consequently gave higher values of dielectric constant.

5.2 Circuit

5.2.1 Gain vs frequency curves

In Section 4.4 the gain versus frequency plots were reported.

The circuit shown in Figure 3 is a second-order RC active filter (lowpass) with a voltage transfer function given by:

$$-\frac{V_o}{V_i} = \frac{\{R_1 R_2 C_1 C_2\}}{s^2 + \{(R_1 C_1)^{-1} + (R_2 C_1)^{-1}\} s + (R_1 R_2 C_1 C_2)^{-1}}$$

$$= \frac{w^2}{s^2 + \frac{w}{Q} s + w^2} \qquad\qquad 5.1.1$$

By coefficient matching:

$$w^2 = (R_1 R_2 C_1 C_2)^{-1} \qquad\qquad 5.1.2$$

Conclusions and recommendations   65

$$\frac{w}{Q} = \frac{\left\{ -\dfrac{1}{R_1} + -\dfrac{1}{R_2} \right\}}{C_1} \qquad \qquad 5.1.3$$

These equations easily reduce to yield the following values

$$R_{1,2} = \frac{1}{2wC_2Q} \{1 \,\overset{+}{-}\, (1 - 4Q^2C_2)/C_1\}^{-1} \qquad 5.1.4$$

The above equations enable one to design for a particular ratio. In this case $C_1/C_2 = 4Q^2$ was used.

The theoretical-ideal curve is obtained using equation 5.1.1 which assumes that the capacitors are lossless.

5.2.2 Analysis of active filter with "lossy" capacitors

Incorporating the "lossyness" of the capacitors by G_a and G_b for the large and small area capacitors respectively one obtains the following modified equation for the transfer function:

$$\frac{V_4}{V_1} = \frac{\dfrac{G_1 G_2}{C_1 C_2}}{s^2 + s\left\{\dfrac{G_1 + G_2 + G_a}{C_1} + \dfrac{G_b}{C_2}\right\} + \left\{\dfrac{G_b[G_1 + G_2 + G_a]}{C_1 C_2} + \dfrac{G_1 G_2}{C_1 C_2}\right\}}$$

$$5.2.1$$

The plot obtained using the above is termed the theoretical-lossy curve. This curve should in principle coincide with the measured gain versus frequency curve but, as seen in Figures 26-29, there is a differnce between the two. A new model was created by incorporating the frequency dependence of the conductance of each of the dielectrics.

Conclusions and recommendations   66

$$G_a = G_{dc}(1 + K_a w) \qquad\qquad 5.2.2$$

where,

G_a is the conductance of the large capacitor fabricated from
   the high-K dielectric,

G_{dc} is the value of the asymptote shown in figure 25,

K_a is the slope of the graph, and

w is the angular frequency

With this modification to the gain equation, the theoretical-lossy and the measured curves correlate very well if measurement accuracy is taken into account. This is illustrated in Figure 34.

Appendices 1 and 2 show the detailed analysis of a lossy dielectric and the analysis of the active filter with "lossy" capacitors.

A similar procedure was followed for the bandpass filter for which the transfer function is as follows:

$$\frac{V_o}{V_i} = \frac{sC_2G_1(1 + G_5/G_4)}{s^2C_1C_2 + sG_1C_2 + G_2G_3G_5/G_4} \qquad\qquad 5.2.3$$

The gain versus frequency plot is shown in Figure 35.

GAIN VS FREQUENCY
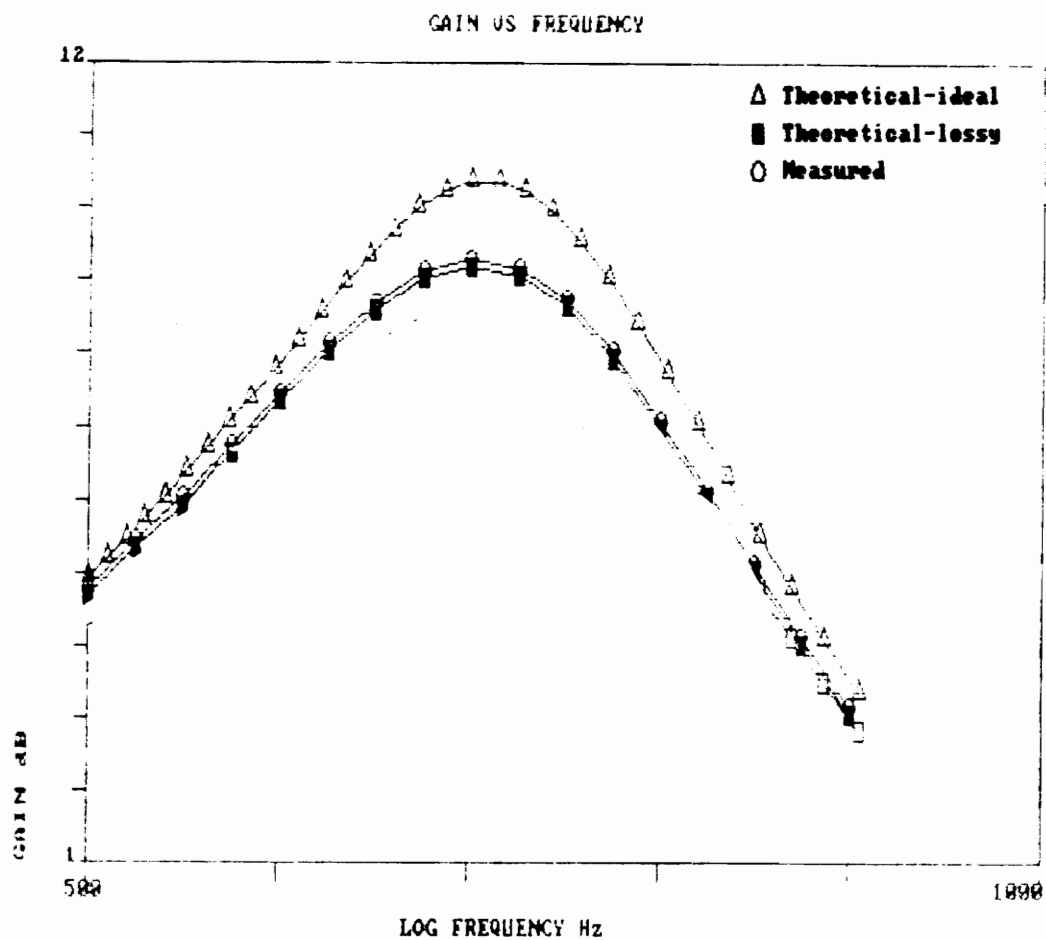
Figure 34. Gain vs frequency curves, showing close
correlation between theoretical-lossy and
measured curves for lowpass RC active filter

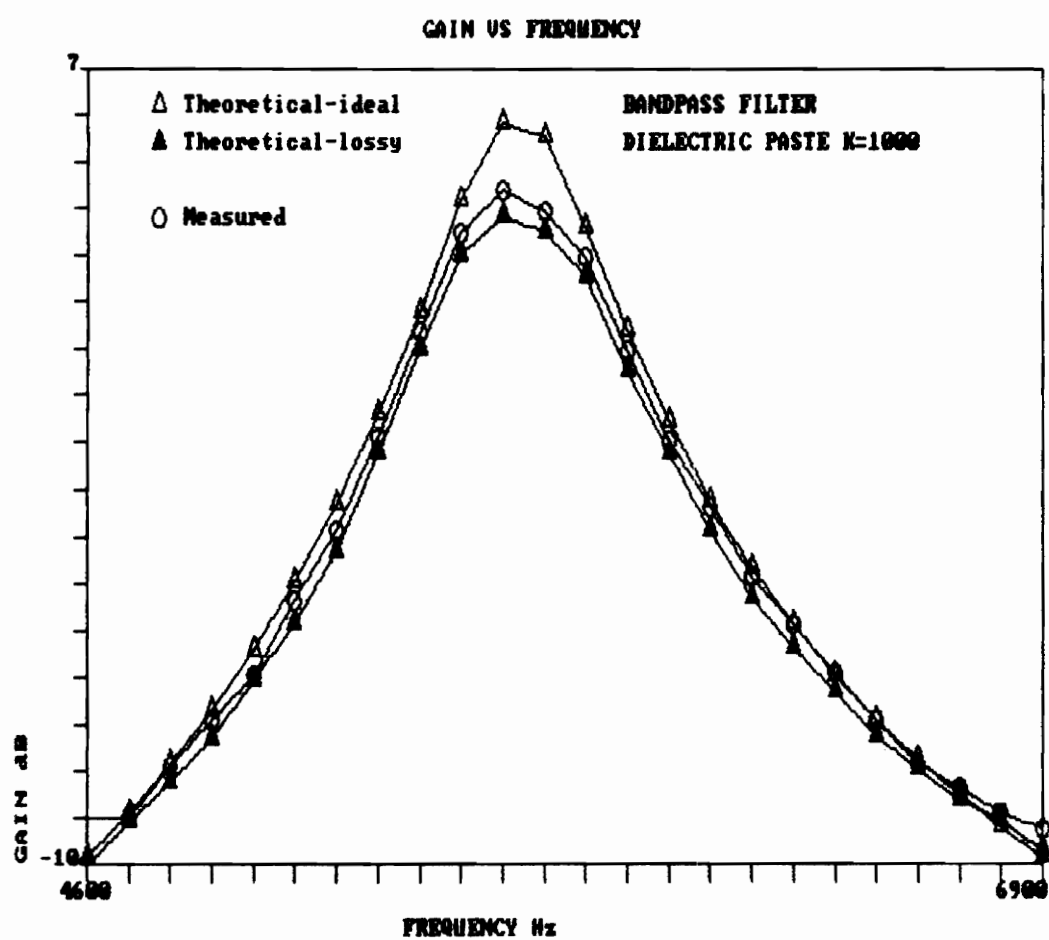Conclusions and recommendations   68

Figure 35.   Gain vs frequency curves for bandpass RC active
             filter

Conclusions and recommendations   69

CHAPTER 6. CONCLUSIONS AND RECOMMENDATIONS

6.1 Conclusions

The main objectives of this research were to examine the electrical characteristics of thick-film capacitors and then to study the performance of these capacitors when buried in a multilayer circuit. The circuit chosen for this project was an RC active filter.

The important results of this study are:

(i)   conductor/dielectric interactions play a major role in the performance of thick-film capacitors,

(ii)   high-K dielectrics have a porous interconnected microstructure and are generally much more lossier than low-K dielectrics,

(iii)   silver migration is more prevalent in high-K materials,

(iv)   the accuracy in the measuement of thickness of dielectric and substrate camber have a large effect on the calculated dielectric constants,

(v)   quality of capacitors was evaluated via performance of the circuit,

(vi)   an analysis was developed to predict center frequency and quality factor utilizing frequency dependence of capacitor losses.

In summary, this study verifies that high-K thick-film capacitors can be used as components in active filter circuits, and can be accurately modelled if their losses are taken into account.

6.2 Recommendations

The following recommendations are made for further study:

(i)   the materials can be characterized at lower firing temperatures, to see if there is an improvement in performance,

(ii) instead of firing each dielectric layer separately, they could be co-fired,

(iii) oscillators and other analog circuits operating at higher frequencies can be studied, thereby utilizing the fact that capacitors are smaller in value at 100 KHz and above.

APPENDIX 1

ANALYSIS OF ACTIVE FILTER WITH "LOSSY" CAPACITORS

Nodal analysis of the lowpass RC active filter shown
in Figure 36 yields:

<u>Node 2:</u> $(G_1 + G_2 + G_a + sC_1)V_2 - G_1 V_1 - G_2 V_4 - (G_a + sC_1)V_4 = 0$

$(G_1 + G_2 + G_a + sC_1)V_2 - G_1 V_1 - (G_a + G_2 + sC_1)V_4 = 0$ -- A1

<u>Node 3:</u> $V_4(G_2 + G_b + sC_2) - G_2 V_2 = 0$ -- A2

<u>From 2</u>

$$V_2 = V_4(1 + \frac{G_b}{G_2} + s\frac{C_2}{G_2})$$

<u>substitute in 1</u>

$(G_1 + G_2 + G_a + sC_1)(G_2 + G_b + sC_2)V_4/G_2 - (G_a + G_2 + sC_1)V_4$

$= G_1 V_1$

$\{(G_1 + G_2 + G_a + sC_1)(G_2 + G_b + sC_2) - G_2(G_a + G_2 + sC_1)\}V_4$

$= G_1 G_2 V_1$

$(G_1 + G_2 + G_a)(G_2 + G_b) - G_2(G_a + G_2) + s\{[G_1 + G_2 + G_a]C_2$

$+ [G_2 + G_b]C_1 - G_2 C_1\} + s^2 C_1 C_2 = G_1 G_2 V_1/V_4$

$G_b(G_1 + G_2 + G_a) + G_2 G_1 + s\{C_2(G_1 + G_2 + G_a) + G_b C_1\}$

$+ s^2 C_1 C_2 = G_1 G_2 V_1/V_4$

$$\frac{V_4}{V_1} = \frac{\frac{G_1 G_2}{C_1 C_2}}{s^2 + s\{\frac{G_1 + G_2 + G_a}{C_1} + \frac{G_b}{C_2}\} + \{\frac{G_b[G_1 + G_2 + G_a]}{C_1 C_2} + \frac{G_1 G_2}{C_1 C_2}\}} \quad A3$$
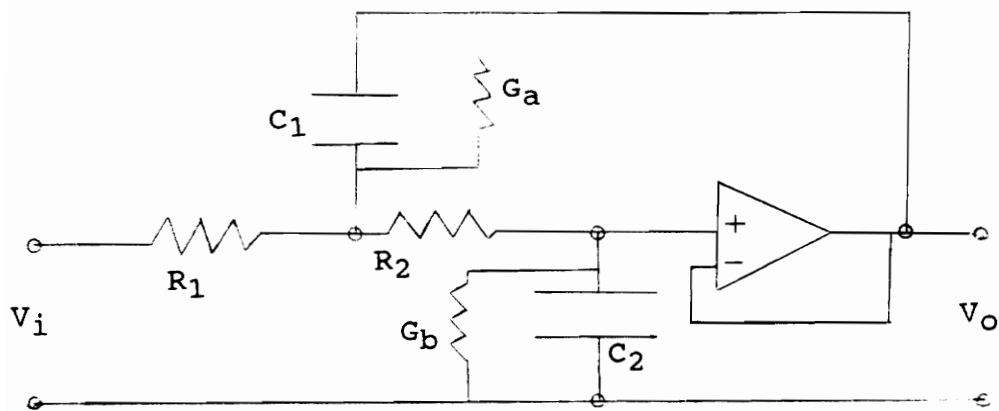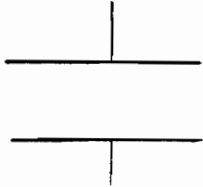
Figure 36. Circuit diagram of lowpass RC active filter
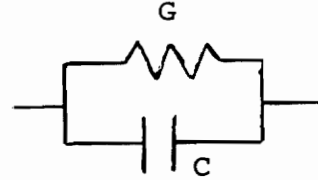with the capacitor losses included

APPENDIX 2

ANALYSIS OF LOSSY DIELECTRIC

Ideal capacitor   Leaky Capacitor

$$i = V(jwC^*) = jwVC_o(\ddot{E}' - j\ddot{E}'') = VwC_o\ddot{E}'' + jVwC_o\ddot{E}'$$

where,

$$C = C_o\ddot{E}'$$

$$G = wC_o\ddot{E}''$$

$$\ddot{E}' - \ddot{E}'' = \text{complex permittivity}$$

$$= \ddot{E}_o \text{x complex dielectric constant } (k' - jk'')$$

$$C_o = \frac{\ddot{E}_o A}{d}$$

Thus in equivalent circuit $G = wC_o\ddot{E}''$, $C = \ddot{E}'C_o$

Implies that $G \longrightarrow 0$ at $w = 0$

Let
$$G \longrightarrow G_{DC} \text{ at } w = 0$$

Then, $G \longrightarrow G_{DC} + wC_o\ddot{E}''$

Frequency response is shown in Figure .

For "good" dielectric
$$G_{DC} \sim 0$$
and,

Dissipation factor (DF) is given by:

$$DF = \frac{\ddot{E}''}{\ddot{E}'}$$

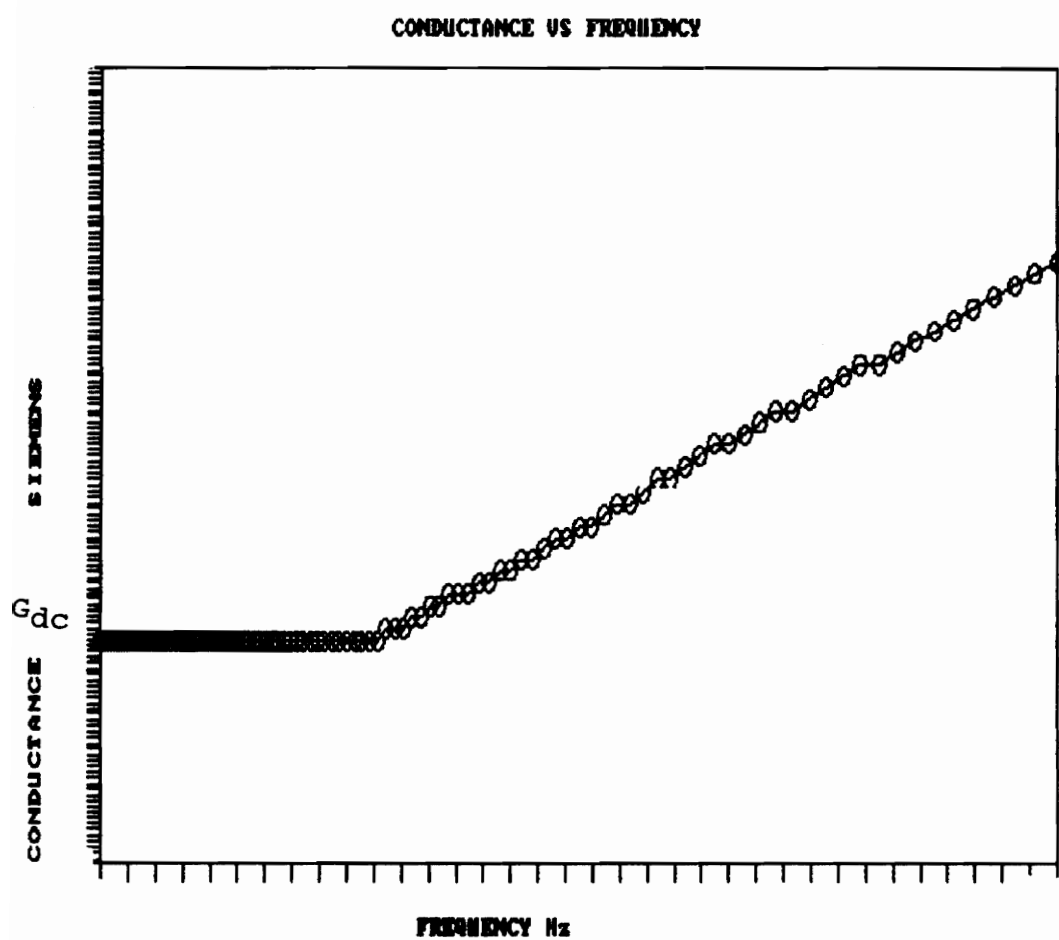CONDUCTANCE VS FREQUENCY

Figure 37. Typical conductance vs frequency plot of
high-K capacitor

BIBLIOGRAPHY

1.   M. Kahn, "Multilayer ceramic capacitors - materials and manufacture", Technical information AVX Corp., May, 1981.

2.   B.E. Taylor and S.T. Joslin, "Dielectric/conductor interactions and their effect on performance", Proc. Intl. Soc. for Hybrid Microelectronics, pp. 30-46, 1986.

3.   B.E. Taylor and W.A. Craig, "Thick-film Pd/Ag conductors: processing and performance study", Proc. Intl. Soc. for Hybrid Microelectronics Proc., pp. 124-131, 1986.

4.   M.L. Kummel, "A screenable high dielectric constant capacitor system for commercial circuit applications", Proc. 22nd Electronic Comp. Conf., pp 124-133, 1972.

5.   D.A. Mclean, "Dielectric materials and capacitor miniaturization", IEEE Trans., Vol. PMP-3, # 4, pp 163-169, Dec. 1967.

6.   C.A. Harper, Handbook of thick-film hybrid microelectronics, McGraw-Hill, New York, 1974.

7.   P.J. Holmes and R.G. Loasby, Handbook of thick-film technology, Electrochemical Pubs. Ltd., 1976.

8.   Z.H. Meiksin, Thin and thick-films for hybrid microelectronics, Lexington Books, Mass., 1976.

9.   W. Worobey, "Tantalum thin-film RC circuit technology

for a universal active filter", IEEE Trans., Vol. PHP-12, # 4, pp 276-282, Dec. 1976.

10. Bell Telephone Laboratories, The physical design of electronic systems, Vol. 3, Integrated devices and construction technology, pp 223-227, Prentice Hall, Englewood Cliffs, N.J., 1971.

11. M. Probstein, "A switchable active filter hybrid", IEEE Trans., Vol. PHP-12, # 3, Sept., 1976.

12. W.R. Bratschun, "Glass-passivated thick-film capacitors for RC circuits", IEEE Trans., Vol. PHP-12, # 3, pp 194-201, Sept., 1976.

13. A. Herczog, "Application of glass-ceramics for electronic components and circuits", IEEE Trans., Vol. PHP-9, pp 167-172, Dec., 1973.

14. K.B. Cook, "The hybrid integration of a multistage active bandpass filter/amplifier", IEEE Trans., Vol. PHP-12, # 4, pp 336-350, Dec. 1976.

15. T.M. Foster, "Thick-film techniques for microwave integrated circuits", IEEE Trans., Vol. PHP-10, # 12, pp 88-94, June, 1974.

16. G.S. Moschytz, "Gain-sensitivity product - A figure of merit for hybrid-integrated filters using single operational amplifiers", IEEE J., Vol. SC-6, # 3, pp 103-110, June, 1971.

17. A.A.R. Riad, EE 4200 class notes, VPI & SU, 1987.

18. T. Ihochi, "Screened multilayer ceramics for thick-film

hybrids", IEEE Trans., Vol. PHP-10, pp 115-119, June, 1974.

19. R.G. Loasby, "Aspects of multilayered thick-film hybrids", Solid State Technology, Vol.19, pp 56-59, May, 1971.

20. J.M. Herbert, "Ceramic dielectrics and capacitors", Electrocomponent Science Monographs, Vol. 6, pp 234-239, 1973.

21. I.K. Yoo, L.C. Burton and F.W. Stephenson, "Electrical conduction mechanisms of barium-titanate based thick-film capactors", IEEE Trans., Vol. CHMT-10, # 2, pp 274-282, June, 1987.

22. I.K. Yoo, "Degradation mechanisms of barium-titanate based thick-film capacitors", MS Thesis, VPI & SU, 1986.

23. W.J. Minford, "Accelerated life testing and reliability of high-K multilayer ceramic capacitors", IEEE Trans., Vol. CHMT-5, # 3, pp 114-121, Sept., 1982.

24. C. Huang, P. Bless and S.J. Stein, "High reliability thick-film dielectrics", ISHM Proc., pp. 433-440, 1984.

25. F.W. Stephenson (Ed.), RC active filter design handbook, Wiley, New York, 1985.

26. P. Bowron and F.W. Stephenson, Active filters for communications and instrumentation, McGraw-Hill, London, 1979.

27. K. Schlozhauer and K. Singhal, "Influence of capacitor

losses on the Q of active filters", Proc. IEEE, 61, pp 1662-1663, 1973.

28. T. Wiktorczyk, "Mechanisms of dielectric polarization in $Al-D_yO_3-Al$ thin-film sandwiches", IEEE 2nd Intl. Conf. on conduction and breakdown in solid dielectrics, pp 222-231, 1986.

29. P.L. Kirby, "Thick-film advances simplify complex hybrid module design", Electron. Eng., 48, pp 35-38, 1976.

30. P. Johnson, "Software for calculation of effective capacitance", Electronic Materials Lab., VPI & SU, 1987.

CURRICULUM VITAE

Raj Reddy was born on February 2, 1961 in Bangalore, India. He attended Faraday High School in London, England. He was awarded the Higher National Diploma in Production Engineering in March, 1983. He then transferred to University of Wales, U.K., where he received his BSc (Honours) degree in Mechanical Engineering in June of 1985. In the fall of 1985 he enrolled at Virginia Tech to pursue his MS degree in Electrical Engineering.

Raj Reddy